INFORMATION TO USERS

This manuscript has been reproduced from the microfilm master. UMI films the text directly from the original or copy submitted. Thus, some thesis and dissertation copies are in typewriter face, while others may be from any type of computer printer.

The quality of this reproduction is dependent upon the quality of the copy submitted. Broken or indistinct print, colored or poor quality illustrations and photographs, print bleedthrough, substandard margins, and improper alignment can adversely affect reproduction.

In the unlikely event that the author did not send UMI a complete manuscript and there are missing pages, these will be noted. Also, if unauthorized copyright material had to be removed, a note will indicate the deletion.

Oversize materials (e.g., maps, drawings, charts) are reproduced by sectioning the original, beginning at the upper left-hand corner and continuing from left to right in equal sections with small overlaps. Each original is also photographed in one exposure and is included in reduced form at the back of the book.

Photographs included in the original manuscript have been reproduced xerographically in this copy. Higher quality 6" x 9" black and white photographic prints are available for any photographs or illustrations appearing in this copy for an additional charge. Contact UMI directly to order.

UMI

A Bell & Howell Information Company
300 North Zeeb Road, Ann Arbor MI 48106-1346 USA
313/761-4700 800/521-0600

UNIVERSITY OF CALIFORNIA, SAN DIEGO

Observations of Seafloor Evolution on a Natural Barred Beach

A dissertation submitted in partial satisfaction of the
requirements for the degree Doctor of Philosophy
in Oceanography

by

Edith L. Gallagher

Committee in charge:

Robert T. Guza, Chairman
Joseph R. Curray
Steve Elgar
Jules S. Jaffe
Daniel B. Olfe
Richard J. Seymour
Bradley T. Werner

1996

The dissertation of Edith L. Gallagher is approved, and it is acceptable in quality and form for publication on microfilm:

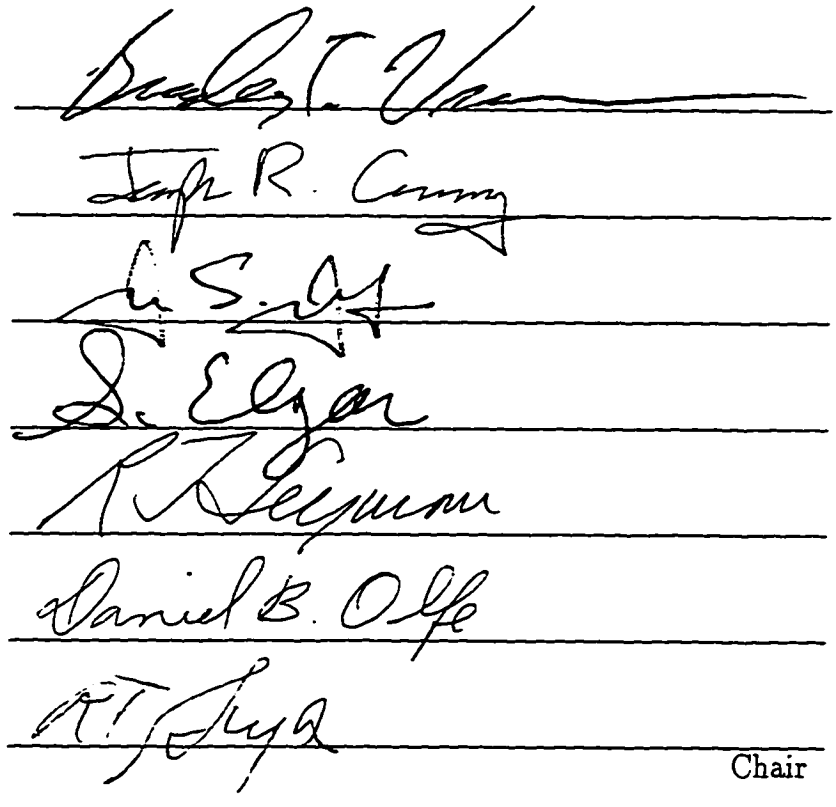

Chair

University of California, San Diego

1996

To my father who taught me so many
wonderful things while I was growing up.

To Peter who teaches me new things everyday.

To Henry K. Gallagher, the newest member of the family.
Maybe I can share some of this with you.

TABLE OF CONTENTS

LIST OF FIGURES

LIST OF TABLES

ACKNOWLEDGEMENTS

I would first like to thank Steve Elgar for asking me to join this project and supporting me from beginning to end. I would also like to thank Bob Guza for taking on the job as my thesis advisor. Working with Steve Elgar and Bob Guza has been an experience I will never forget. Their wild passion and unbridled enthusiasm for science, their remarkable wisdom and clarity and their seemingly endless energy are mind-boggling. I can only hope that some of these qualities have rubbed off on me and I hope they do not regret becoming dirt weenies.

I would also like to thank the rest of my committee. Dick Seymour got me going in sediment transport and Brad Werner has kept my enthusiasm for sand going. Jules Jaffe has always been full of helpful comments, suggestions and advice as well as wit and good humor. I would also like to thank Dr. Curray and Dr. Olfe for valuable comments, suggestions and questions. Bill Dally, at FIT, first introduced me to nearshore processes. He encouraged and helped me to continue in my studies of beaches. I then spent a great summer at WHOI working with Dave Aubrey who suggested Scripps. Lots of thanks go to Bill and Dave.

The group here at CCS who work with Elgar and Guza are, in some ways, the most deserving of thanks. Without this incredibly talented group of engineers and scientists, this research would not have been possible. AND they are all fun to hang out with! Thank you, Mike Clifton, Bill Boyd, Brian Woodward, Kimball Millikan, Britt Raubenheimer, Tom Herbers, and Jerry Wanetick.

The great friendships I have made (and continued) at Scripps have been numerous. I will begin by thanking those with whom I have shared a home: Grieg Steward, Heidi Dewar, Tom Boyd, Tim Welch (with honorable mention to Lisa and Kirsten), Deena Mallareddy, Will Von Reis, Susan LaGreca, and Megan Flanagan. Next I want to thank those with whom I have shared an office: Karl Rieder and my confidante, roll model, and big sister Michele Okihiro (and Mele Okihiro Johnson). Finally I want to acknowledge the others with whom I would have gladly shared

space: Steve Katz, Josefina Martinez, Greg and Anne Bullard, Wayne Crawford. You have been my family here and my memories of graduate school will always be sweet because of you.

I want to thank my mother and father. The unique combination of encouragement, support, freedom, and passion that you have both given me makes me absolutely sure that you are the best parents in the world. I did not go to graduate school because I had to or because I should, I did it because I wanted to and I could, that is what you have given me. I hope I do as well with my children.

Finally I want to thank Peter. Thank you for tolerating my absences and waiting for me. Thank you for making my life complete. I love you.

The text of Chapter I, in full, is a reprint of the material as it appears in Marine Geology. The dissertaion author, Edith L. Gallagher, was the primary researcher. The role of the co-authors, S. Elgar, W. Boyd, R.T. Guza, and B. Woodward consisted of guidance and advice, suggestions, critical discussion, and editorial comments on the manuscript.

VITA

June 8, 1963	Born, Philadelphia, Pennsylvania
1988	B.S. Florida Institute of Technology, Melbourne, FL
1988–1989	Research Assistant, General Electric CRD, Niskayuna, NY
1989–1991	Sea Grant Trainee, University of California, San Diego
1991–1996	Research Assistant, University of California, San Diego
1996	Doctor of Philosophy University of California, San Diego

PUBLICATIONS

Gallagher, E.L., W. Boyd, S. Elgar, R.T. Guza, and B. Woodward, Performance of a Sonar Altimeter in the Nearshore, *Marine Geology* **133**, 241–248, 1996.

Gallagher, E.L. and R.J. Seymour, Oscillatory bedload transport studies by imaging of tracers. International Conference on Coastal Engineering, Venice, American Society of Civil Engineers, pp 2084–2094, 1992.

Gallagher, E.L., R.J. Seymour and D.B. King, Bedload transport measurement by imaging of tracers. Proceedings Coastal Sediments '91, Seattle, American Society of Civil Engineers, pp 717–725, 1991.

FIELDS OF STUDY

Major Field: Oceanography

Studies in Nearshore Processes.
Professors S. Elgar (WSU), R.T. Guza, D.L. Inman and Dr. S.A. Jenkins

Studies in Linear and Nonlinear Waves.
Professors M.C. Hendershott, R. Pinkel, R.T. Guza and S. Elgar (WSU)

Studies in Geophysical Data Analysis.
Professors D. Agnew and R.L. Parker

Studies in Fluid Mechanics.
Professor C.D. Winant

Studies in Geomorphology and Marine Geology.
Professors B.T. Werner, J.R. Curray, W.H. Berger and T. Drake (North Carolina State University)

ABSTRACT OF THE DISSERTATION

Observations of Seafloor Evolution on a
Natural Barred Beach

by

Edith L. Gallagher
Doctor of Philosophy in Oceanography
University of California, San Diego, 1996
Professor Robert T. Guza, Chair

Waves, currents, and morphology were measured nearly continuously for more than 2 months at 9 locations along a cross-shore transect extending from the shoreline to 4-m water depth. Changes in seafloor location were measured with newly developed sonar altimeters which can locate the seafloor even in the surf zone during storms. During the deployment the sand bar moved 130 m offshore (primarily when the offshore significant wave height exceeded about 2 m), with 1.5 m of erosion near the initial location of the bar crest and 1 m of accretion offshore. Onshore bar migration was observed for low-energy conditions. An energetics-type sediment transport model driven by locally measured near-bottom currents predicts the observed offshore bar migration accurately, but the slight onshore migration observed during low-energy wave conditions is not well modeled. The predicted offshore bar migration is driven primarily by gradients in suspended sediment transport associated with quasi-steady, near-bottom, offshore flows. These strong (> 50 cm/sec) currents, possibly enhanced by intensified wave breaking near the bar crest, are predicted to cause erosion on the shoreward slope of the bar and deposition on the seaward side. The feedback between the morphology, waves, circulation, and sediment transport thus forces offshore bar migration when waves are large enough to break on the bar. During lower energy events and onshore migration the skill

of the model is reduced. This may be the result of phase lags between sediment suspension in the lee of bedforms. Megaripples (not accounted for in the transport model) with heights of O(20 cm) migrating at speeds as high as 100 cm/hr were often observed with a coherent array of altimeters located in the trough shoreward of the sand bar.

Chapter I

Performance of a Sonar Altimeter in the Nearshore

Abstract

A 1 MHz sonar altimeter with automatic gain control is shown to provide accurate estimates of the distance between the instrument and the seafloor. Laboratory experiments indicate that distance estimates degrade slightly when the bottom is rough or sloped and when sediment is suspended in the water column. Results from field tests, both within and seaward of the surf zone, show some degradation owing to a combination of suspended sediment and bubbles, bed undulations, and perhaps the dynamic nature of the sand bottom under waves. Seaward of the surf zone the bottom can be located within ± 2 cm nearly continuously, whereas inside the surf zone the bottom can be located only intermittently and the accuracy decreases to ± 3 cm. A 300 m long cross-shore transect of 16 altimeters was deployed from the shoreline to about 4 m depth for 3 months in summer-fall 1994 near Duck, NC. Results show that the altimeters are robust and can usually provide estimates of the seafloor position every few minutes even in the surf zone during large storms.

1. Introduction

Sonar altimeters can be used to estimate the location of the seafloor by measuring the time for an acoustic pulse to travel to the seafloor and back, and converting to a distance with the theoretical sound speed. Sonar altimeters mounted on fixed frames have been used to investigate nearshore bedforms (Dingler at al. 1977, Dingler & Clifton 1984), to measure accretion and erosion in intermediate water depth (8 m) (Wright et al. 1986), and to estimate the height of current meters above a sandy continental shelf (Grant et al. 1983). Owing to the severe attenuation and scattering of the sonar beam by suspended sand and bubbles associated with breaking waves in very shallow water, sonar altimeters mostly have been deployed seaward of the surf zone. Even in water 8 m deep, the performance of sonar altimeters can be poor during storms (Green & Boon 1988). In the present study, laboratory and field tests of a sonar altimeter that can locate the seafloor with uncertainties of a few centimeters through bubbly and turbid surf zone waters are described. Automatic gain control (AGC) is used to accommodate large fluctuations in the acoustic propagation properties of the water column, thus improving the bottom-locating capability of the altimeter. A post-processing algorithm rejects spurious sonar returns from suspended sand and bubbles. Preliminary results from a field deployment demonstrate that the altimeter can monitor nearshore bathymetric evolution on both relatively small (megaripples, lengths of 1 - 10 m and heights of 10 - 50 cm) and large (sand bars, lengths of 100 - 200 m and heights of a few m) spatial scales for several months with little maintenance.

2. The Altimeter

The altimeter consists of a 2.54 cm diameter transducer (V302-SB Videoscan immersion transducer manufactured by Panametrics, Inc.) and its electronics housed in a 7 cm diameter, 35 cm long PVC tube. The transducer beamwidth of approximately 3.4° results in a 6 cm diameter footprint at 1.0 m range. A 1

MHz acoustic pulse (duration 10 μsec) is transmitted 25 times per second, with return echoes detected after each pulse. Because the transducer vibrates after the pulse is sent, and early reflections can be noisy, the incoming signal is blocked for 270 μsec, corresponding to a minimum detectable distance to the sea floor of approximately 20 cm. The maximum range varies from approximately 180 cm in turbid, bubbly water to more than 250 cm in clear water.

The strength of the bottom reflection can vary as the concentration of bubbles and suspended sediment in the water column fluctuates (e.g., with the passage of bores and/or sediment clouds), and thus an altimeter that uses a fixed threshold to detect the bottom echo is ineffective in the surf zone. Using AGC, the instrument gain is adjusted (and applied to the subsequent pulse) to maintain an approximately constant peak voltage regardless of attenuation and scattering in the water column (Figure 1.1). A threshold voltage for detecting the bottom is set just below this constant level, and the travel time of the first return above the threshold (Figure 1.1) is used to calculate the distance to the seafloor (the dependence of sound speed on water temperature, measured with a colocated thermistor, is accounted for in post-processing).

Although bottom location estimates discussed here are based on travel times sampled at 2 Hz, sample rates, threshold voltages, and AGC response characteristics are adjustable. Incorrect estimates of the distance to the bottom can occur when the assumption that the strongest echo comes from the seafloor is violated, when the effects of bubbles on sound speed are not negligible, and when there are very large variations between the successive (25 Hz) return pulses (i.e., successive return pulses are similar in Figure 1.1). A schematic block diagram of the AGC altimeter electronics is shown in Figure 1.2.

3. Laboratory Tests

The altimeter was suspended about 90 cm above the smooth metal bottom of a laboratory tank filled with sea water. The mean distance to the bottom

estimated with the altimeter was within the few mm accuracy of an independent distance estimate and had a resolution (scatter) of ± 1 mm, approximately equal to the acoustic wavelength ($\sim$ 1.5 mm) and close to the theoretical resolution of the instrument ($\sim$ .75 mm). The scatter of the estimates increased to ± 2 mm when a level bed of sand grains (diameter $\sim$ 1 mm) covered the bottom, probably because of the uneven reflecting/scattering surface of the grains.

On a sloping bed, the first return from the bottom could be from the higher portions of the footprint, resulting in an underestimate of the average distance to the bed (Dingler, 1974 and Green & Boon, 1988). Although the shape of artificially steep bedforms is qualitatively reproduced when the altimeter is translated across them (Figure 1.3), the narrow troughs (with widths similar to the 6 cm diameter footprint) are truncated (positions 158 and 175 cm, Figure 1.3) and the narrow peaks are smoothed (positions 148 and 165 cm, Figure 1.3).

The scatter (ie, the thickness of the band of returns from the bottom) was about ± 7.5 mm, compared to ± 2 mm for the flat, compacted sand bed, possibly owing to returns from the vertical extent of the footprint or to a change in the scattering properties of the bed because of dilation of the sand during construction of the ripples. The $\sim$ 2 cm offset error (Figure 1.3) is comparable to the accuracy of the manual surveys (done with a plumb bob suspended from a string).

To determine the effect of suspended sediment on the bottom-detection capability of the altimeter, tests were performed in an elutriator, a cylindrical flow channel in which water is pumped vertically upward to suspend sediment. Tests were performed for a range of sediment grain diameters (0.1-10 mm). Larger grain sizes in suspension degraded the bottom-finding capability relative to smaller grain sizes. When the grain size is comparable to, or larger than, the acoustic wavelength ($\sim$ 1.5 mm), the acoustic pulse will be reflected, as opposed to being scattered from smaller grains (Urick, 1983). Strong reflections from larger grains in the water column are effective at masking the true bottom location.

4. Field Tests

Field tests were conducted seaward of the surf zone in about 3 m water depth near the Scripps Institution of Oceanography. The significant wave height ranged from 38 to 62 cm. Divers observed that the upper layer of sand was often moving in response to wave-orbital velocities and that orbital ripples often covered the seafloor near the altimeter. Divers also observed that scour from the support frame did not extend into the altimeter footprint. Altimeter estimates of the distance to the undisturbed sand bottom had about ±2 cm scatter (0-11 min, Figure 1.4), compared to ±0.5 cm scatter when a smooth metal plate was placed on the sand below the altimeter and leveled by pressing it into the bed (11-30 min, Figure 1.4). After the plate was removed, the scatter of the bottom location estimates (±1 cm) was reduced relative to the scatter from the undisturbed sand (±2 cm), possibly owing to compaction of dilated sand during leveling of the plate. Removal of the plate did not result in relaxation of the 2 cm sand compression. Between minutes 25 and 29 (Figure 1.4) sand was released from a container, suspending sediment in the water column between the altimeter and the plate. There were many false returns from the water column, but the bottom location is still apparent.

The performance of the AGC altimeter was superior to that of a colocated nonAGC altimeter. At best, the nonAGC altimeter accurately located the bottom 85% as often the AGC altimeter. During turbid conditions when the bottom was more difficult to locate, 33% of the AGC altimeter estimates were accurate, compared to 1% of the nonAGC altimeter estimates.

Bottom location estimates for 1.2 days during a surf zone field test (mean water depth from 0 to 150 cm depending on tidal stage) are shown in Figure 1.5. Although breaking-wave induced bubbles and suspended sand produce a large number of errant returns from the water column, the seafloor position is distinguishable as the dark band of dots (width about ±3 cm) between approximately 60 and 80 cm below the fixed altimeter. Most of the errant returns fall between 20 and 25 cm. When the return signal noise floor is similar in magnitude to the

bottom return it may be amplified to the detect threshold through adjustment of the gain by the AGC (Figure 1.1), resulting in an (incorrect) estimate at, or near, the minimum detectable distance, 20 cm. During low tide (eg, day 20.1 - 20.3 and beginning again at day 21.2) the altimeter was above the water surface, producing the 'black snow' of dots with no distinguishable seafloor location.

5. Bottom-Finding Algorithm

Although as many as 70% of the sonar returns can be erroneous, especially in the surf zone, the seafloor is often readily detectable by eye (e.g., Figure 1.5). To routinely process the raw, 2 Hz sonar returns, an algorithm has been developed that provides accurate estimates of the bottom location every 32 seconds. First, a histogram with 2-cm wide distance bins is constructed from 256 s of 2 Hz samples. The distance bin with the most occurrences (excluding bins less than 25 cm, which contain most of the false returns) provides a rough estimate of the distance to the seafloor. The 256-s record is then subdivided into eight 32-s records, and a histogram with 0.5 cm-wide bins (within ± 20 cm of the maximum of the 256-s histogram) is constructed for each. The maxima of the 32-s histograms provide estimates of the distance to the seafloor every 32 s. The estimates of the bottom location used here had a minimum of 5 (100) points in the peak of the 32-s (256-s) histogram. Distance estimates from the bottom-finding algorithm for the surf zone data in Figure 1.5 are shown offset by 25 cm. The parameters used in the algorithm were determined by trial and error using data from the field tests and a subsequent 3-month long field deployment (discussed below). The algorithm only failed during the most energetic conditions in the surf zone.

6. Preliminary Results from a 3-Month Long Field Deployment

For approximately 3 months in summer-fall 1994, 16 AGC sonar altimeters colocated with current meters, pressure gages, and thermistors were deployed

along a cross-shore transect extending from the shoreline to about 4-m water depth near Duck, NC. The altimeters were quite robust, with only one electronic failure. No additional maintenance was required other than occasional cleaning of biological growth and vertical adjustment to keep the altimeters within the operating range (25-200 cm above the seabed).

The elevation of the seafloor (relative to mean sea level) in the surf zone over an 80-day period estimated by one AGC sonar altimeter is shown in Figure 1.6. Between days 56 and 63 the offshore significant wave height reached 4 m and the sand bar moved offshore, resulting in 1.5 m of erosion at this location (cross-shore distance = 220 m in Figure 1.7) and nearly 1 m of accretion further offshore (cross-shore distance = 320 m in Figure 1.7).

The cross-shore transect contained a dense, two-dimensional array of 7 AGC altimeters located in about 2 m water depth (cross-shore distance = 170 m in Figure 1.7). Four days of observations from 3 sonars closely spaced along the cross-shore leg of the array are shown in Figure 1.8. The 20 cm fluctuations during day 59 and 60 were migrating megaripples, and the slopes of the 3 nearly vertical lines connecting the 'troughs' of the bedforms correspond to a cross-shore migration speed of about 30 cm/hr toward the beach.

7. Conclusions

Automatic gain control has improved the ability to estimate the seafloor location with a downward looking 1 MHz sonar altimeter. Coupled with a bottom-finding algorithm, the altimeter can accurately (± 3 cm) estimate the seafloor location about twice per minute, even in the surf zone where energetic breakers and strong currents produce bubbles and dense suspensions of sediment. A field deployment of 16 altimeters near Duck, NC demonstrated that this robust sensor requires little maintenance over several months.

Acknowledgements

This research was supported by the Office of Naval Research (Coastal Dynamics and AASERT graduate student support) and the National Science Foundation (Coastal Ocean Processes program). The Hydraulics Laboratory of the Scripps Institution of Oceanography provided construction and testing facilities. The US Army Corps of Engineers Field Research Facility provided excellent logistical support. Dr. Bradley Werner made valuable comments.

The text of Chapter I, in full, is a reprint of the material as it appears in Marine Geology. The dissertaion author, Edith L. Gallagher, was the primary researcher. The role of the co-authors, S. Elgar, W. Boyd, R.T. Guza, and B. Woodward consisted of guidance and advice, suggestions, critical discussion, and editorial comments on the manuscript.

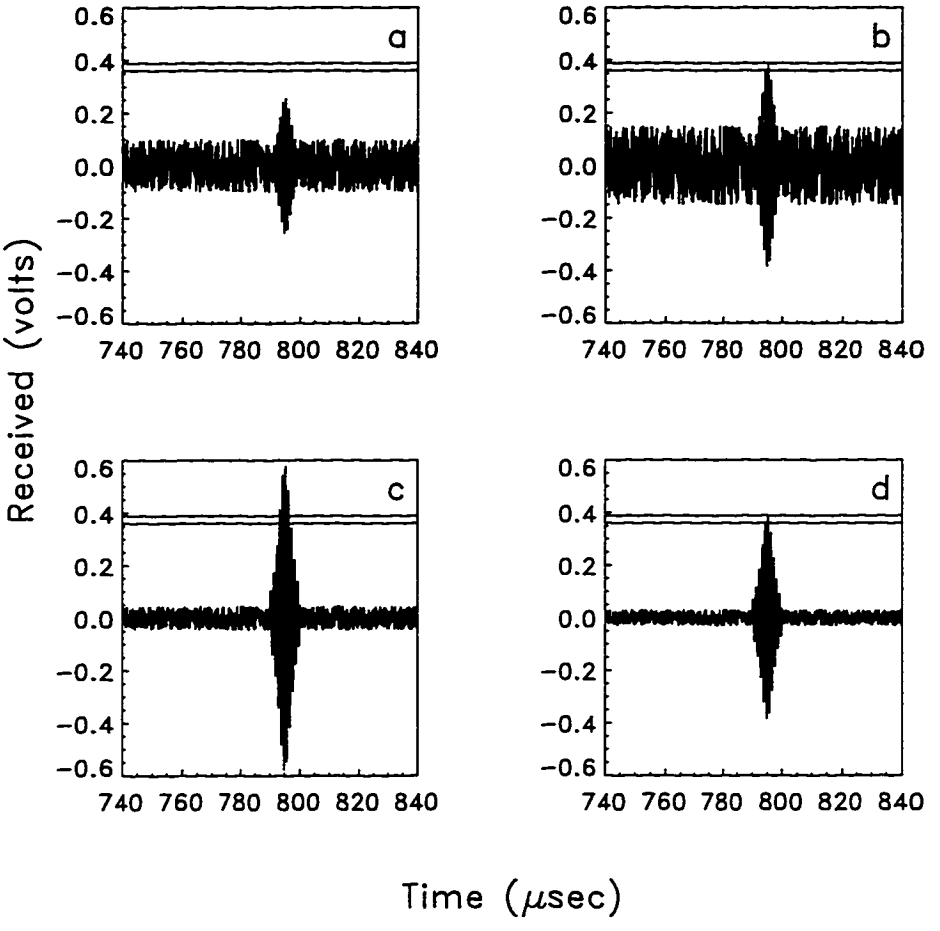

Figure 1.1: Received acoustic signal strength versus time. A pulse (10μs duration) of 1 MHz sound, transmitted by the altimeter at t=0, is reflected from the seafloor 60 cm below and received at t $\sim$ 795μs. A weak return pulse is shown before (a) and after (b) gain adjustment to increase the signal level. A strong reflected pulse received by the altimeter is shown before (c) and after (d) gain adjustment to reduce the signal level. The AGC constant voltage (0.389 V) and the detect threshold voltage (0.361 V) were chosen by trial and error.

Figure 1.2: Block diagram of the automatic gain control (AGC) sonar altimeter circuitry. XPW is the transmitted pulse, RBO is the receiver blank-out pulse, and PAGC is the AGC control pulse.

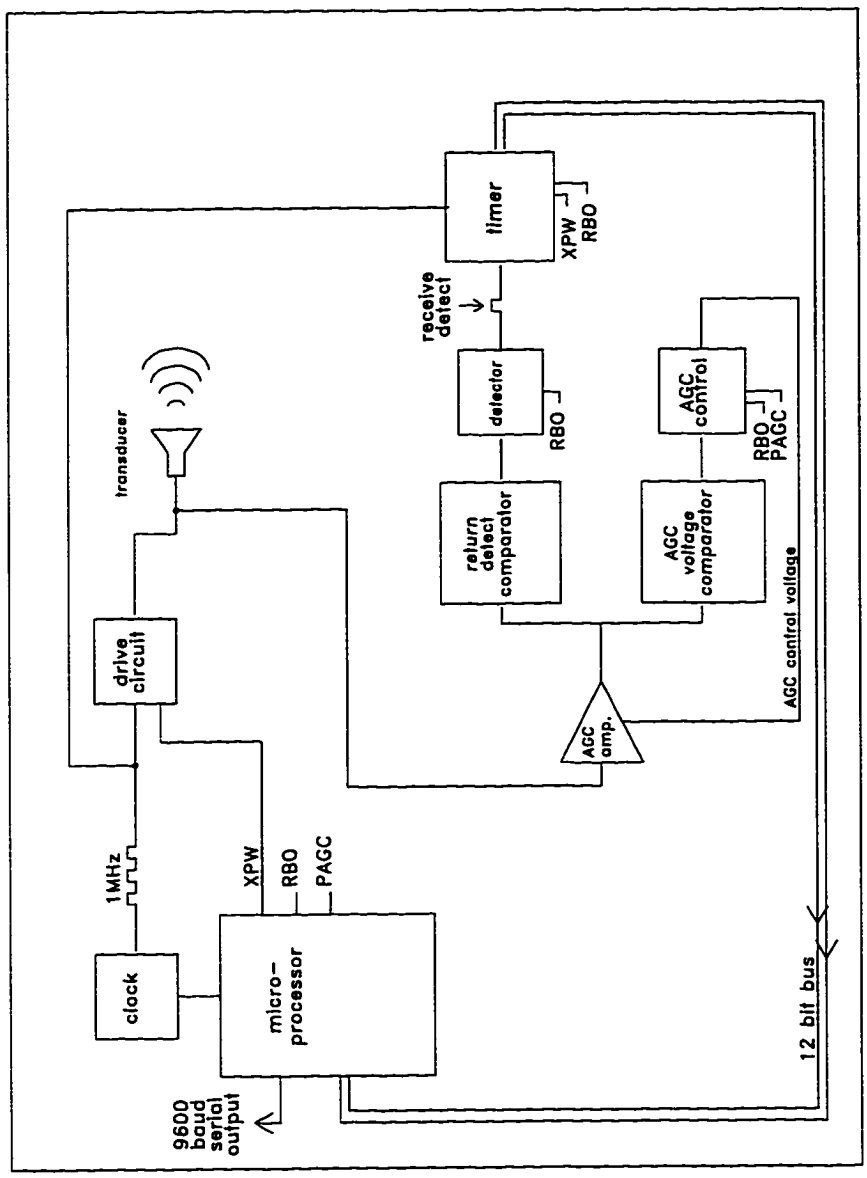

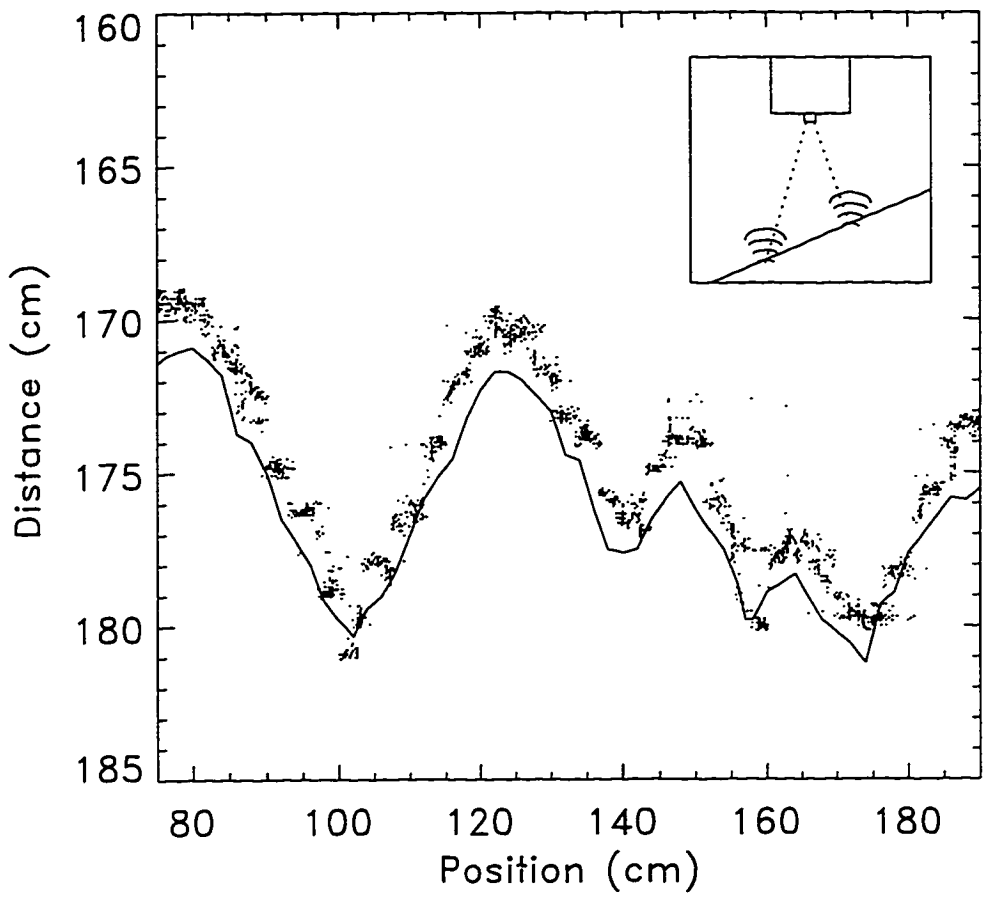

Figure 1.3: Distance of the sonar altimeter above a sand bed versus position along the centerline of a laboratory tank. Each point represents a sonar altimeter estimate and the solid line represents a manual survey (approximately ± 2 cm accuracy). Inset: footprint of altimeter on a sloped surface.

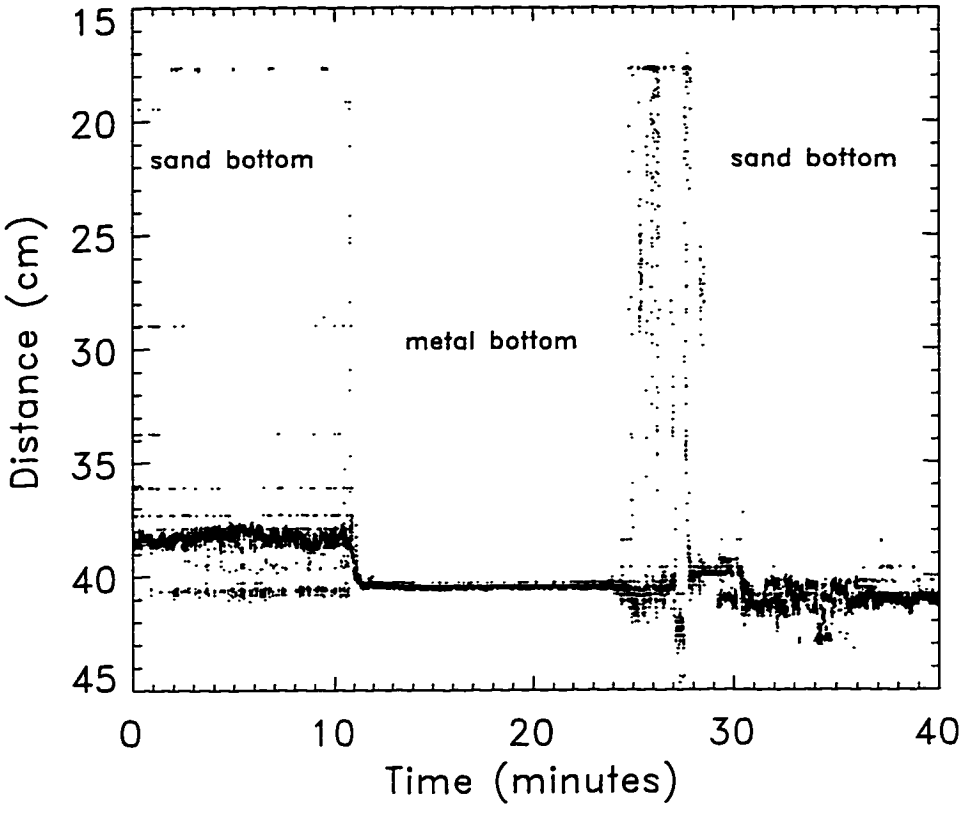

Figure 1.4: Distance of the sonar altimeter above the bed seaward of the surf zone (3 m water depth) versus time. Each point represents an altimeter estimate (every 0.5 s). The seafloor was a natural sand bed from time = 0 until time = 11 min, when a smooth metal plate was leveled on the sand below the altimeter. At time = 25 min a container of sand was emptied above the metal plate, partially filling the water column with suspended sand. The smooth plate was removed at time = 30 min.

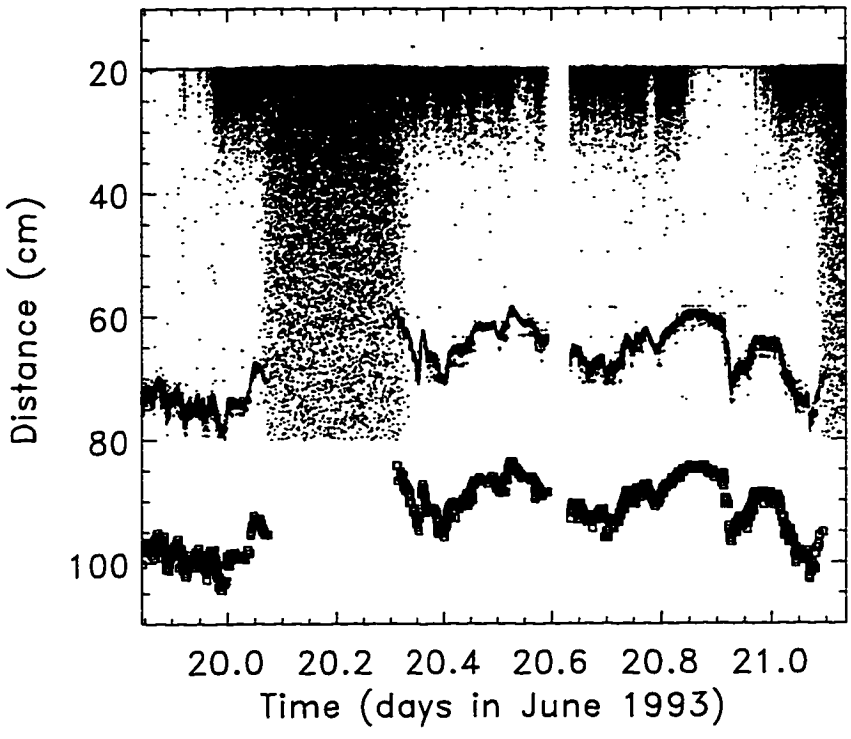

Figure 1.5: Distance of the sonar altimeter above the seafloor in the surf zone versus time. The dots represent raw, altimeter estimates every 0.5 s. The (fluctuating) seafloor position is distinguishable as the dark band of dots between approximately 60 and 80 cm. At low tide (e.g., between about 20.1 and 20.3 days) the altimeter was out of the water, producing the 'black snow' of dots with no distinguishable seafloor location. The squares (offset 25 cm for clarity) represent the 32-s estimates from the bottom-finding algorithm.

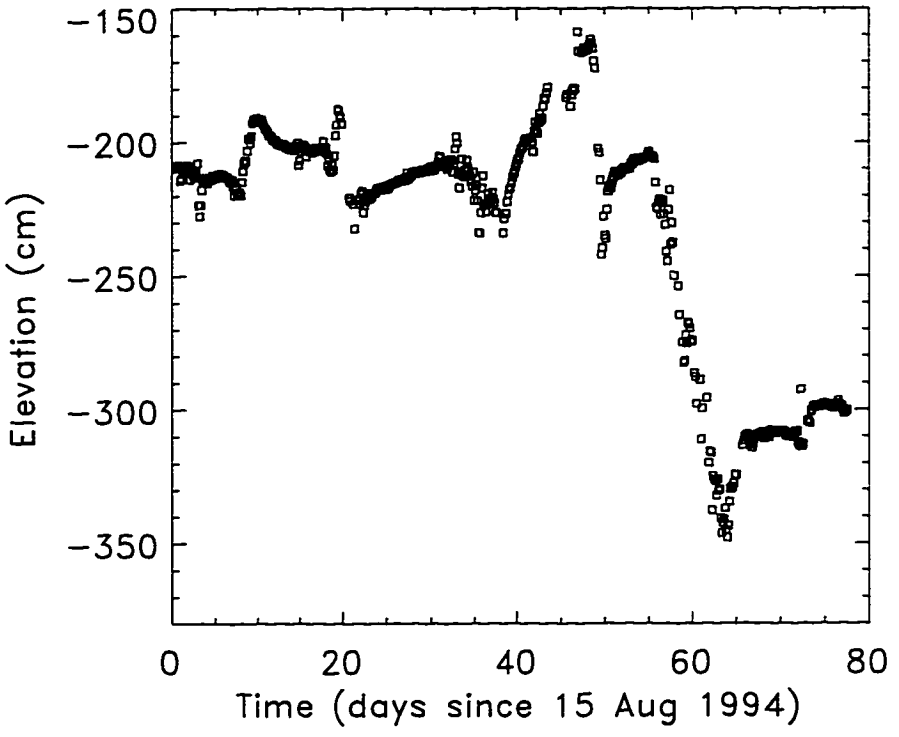

Figure 1.6: Elevation of the seafloor (relative to mean sea level) in the surf zone estimated by a sonar altimeter mounted on a fixed frame near cross-shore position 220 m (see Figure 1.7) versus time. Each symbol is a 3-hr average estimate of the seafloor elevation.

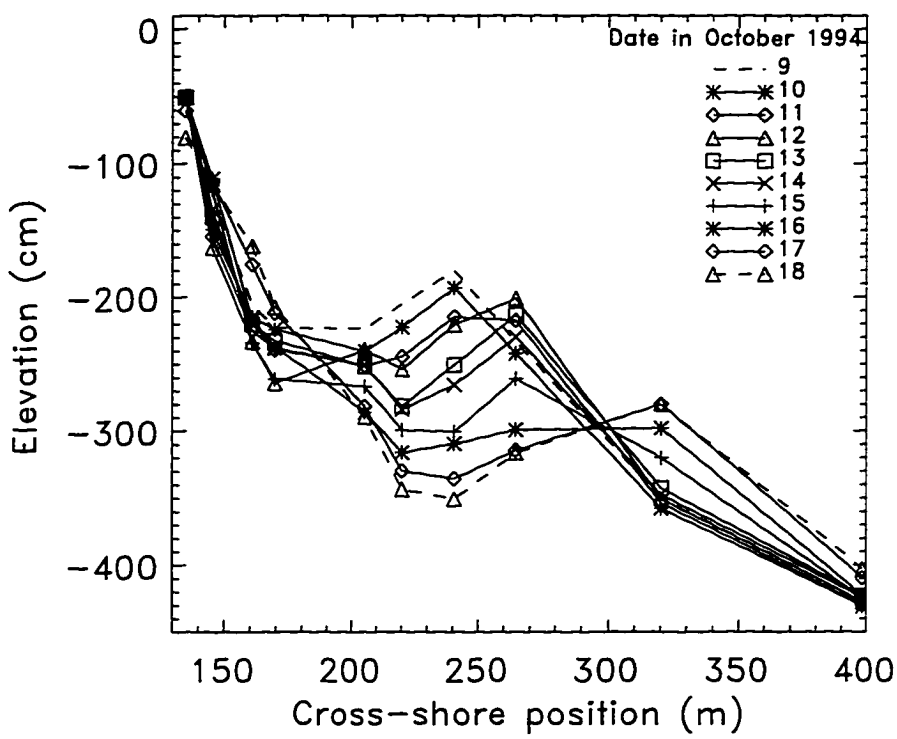

Figure 1.7: Elevation of the seafloor (relative to mean sea level) estimated by sonar altimeters versus cross-shore position. The symbols are 3-hr average elevations (1300-1600 hrs) between days 55 (dashed curve) and 64 (dashed curve with triangles).

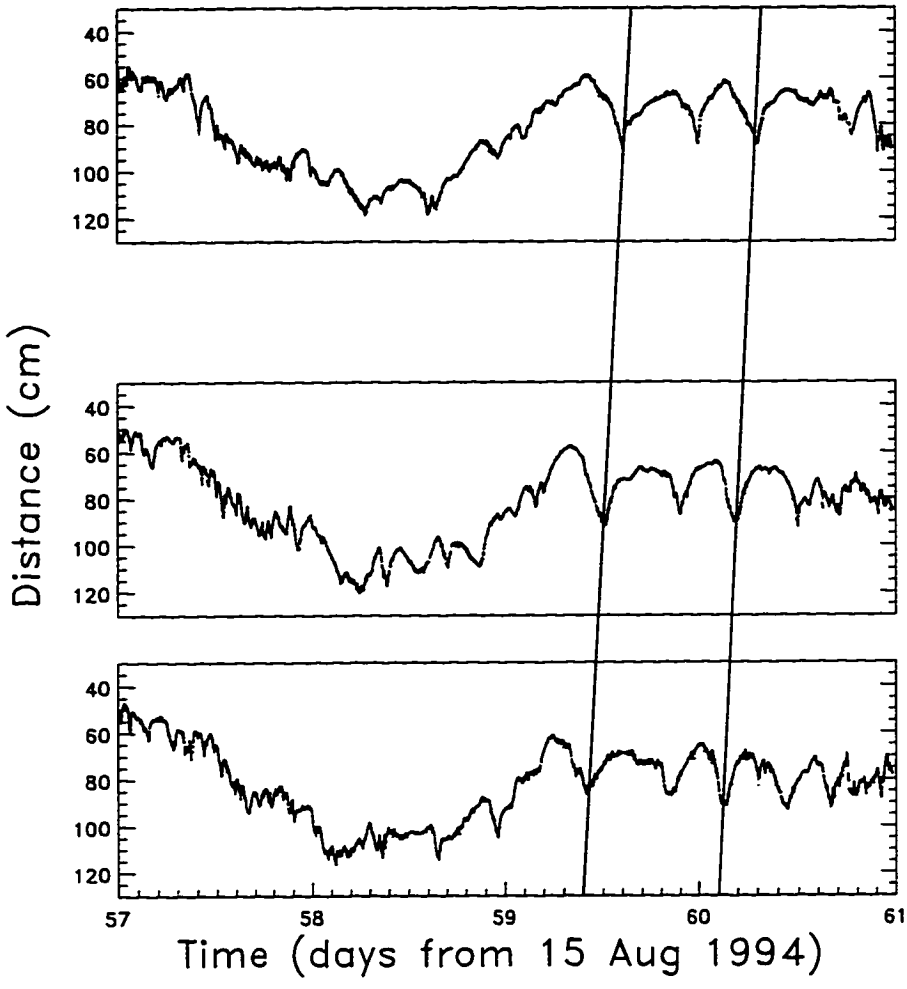

Figure 1.8: Distance of the seafloor below 3 fixed sonar altimeters (located near cross-shore position 170 m, Figure 1.7) versus time. Each point represents a 32-s estimate of the bottom location. The altimeters are separated by 80 cm (upper to middle panel) and 60 cm (middle to lower panel) in the cross-shore direction. The slopes of the 3 nearly vertical lines connecting the 'troughs' of the bedforms suggest a migration speed of about 30 cm/hr toward the beach (along the array axis).

References

Clifton, H.E., Hunter, R.E., and Phillips, R.L., 1971. Depositional structures and processes in the non-barred high-energy nearshore. J. Sed. Pet., 41: 651–670.

Dingler, J.R., 1974. Wave-formed ripples on nearshore sands. Unpubl. Ph.D. thesis, University of California, San Diego, CA., 136 pp.

Dingler, J.R., Boylls, J.C., and Lowe, R.L., 1977. A high-frequency sonar for profiling small-scale subaqueous bedforms. Mar. Geol., 24: 279–288.

Dingler, J.R., and Clifton, H.E., 1984. Tidal-cycle changes in oscillation ripples on the inner part of an estuarine sand flat. Mar. Geol., 60: 219–233.

Grant, W.D., Williams, A.J., Glenn, S.M., Cacchione, D.A., and Drake, D.E., 1983. High frequency bottom stress variability and its prediction in the CODE Region. Woods Hole Oceanographic Institution, Tech. Rep. 83-19, 71 pp.

Green, M.O., and Boon, J.D., 1988. Response characteristics of a short-range, high-resolution digital sonar altimeter. Mar. Geol., 81: 197–203.

Urick, Robert J., 1983. Principles of Underwater Sound. McGraw-Hill, New York, N.Y., 423 pp.

Wright, L.D., Nielsen, P., Shi, N.C., and List, J.H., 1986. Morphodynamics of a bar-trough surf zone. Mar. Geol., 70: 251–285.

Wright, L.D., Boon, J.D., Green, M.O., and List, J.H., 1986. Response of the mid-shoreface of the southern Mid-Atlantic Bight to a "northeaster". Geomar. Lett., 6: 153-160.

Chapter II

Observations of Seafloor Evolution on a Natural Beach

Abstract

Waves, currents, and the location of the seafloor were measured on a barred beach for about 2 months at 9 locations along a 255-m long cross-shore transect extending from 1 to 4 m water depth. The seafloor location was measured nearly continuously, even in the surf zone during storms, with sonar altimeters mounted on fixed frames. A sand bar initially about 60 m from the shoreline moved 130 m offshore (primarily when the offshore significant wave height exceeded about 2 m), with 1.5 m of erosion near the initial location of the bar crest and 1 m of accretion at the final offshore bar location. An energetics-type sediment transport model driven by locally measured near-bottom currents predicts the observed offshore bar migration accurately, but the slight onshore migration observed during low-energy wave conditions is not well modeled. The predicted offshore bar migration is driven primarily by gradients in suspended sediment transport associated with quasi-steady, near-bottom, offshore flows. These strong (> 50 cm/sec) currents, possibly enhanced by intensified wave breaking near the bar crest, are predicted to cause erosion on the shoreward slope of the bar and deposition on the seaward side. The feedback between the morphology, waves, circulation, and sediment transport thus forces offshore bar migration when waves are large enough to break on the bar. Megaripples (not accounted for in the transport model) with

heights of O(20 cm) migrating at speeds as high as 100 cm/hr were often observed with a small coherent array of altimeters located shoreward of the sand bar.

1. Introduction

Sand bars are an important morphologic feature of natural beaches. At many sites, changes in bar position and height are the primary source of beach profile variability (Holman and Sallenger 1993). Bars also significantly effect cross-shore wave transformation and the subsequent profile evolution (Takeda and Sunamura 1987, Seymour 1987, and many others). However, the formation and evolution of sand bars are poorly understood. Holman and Sallenger (1993) review hypotheses for sand bar formation and conclude that both the break-point (Dyhr-Nielsen and Sorenson 1970) and infragravity wave (Holman and Bowen 1982 and references therein) mechanisms may be important. The present work concerns the evolution of a pre-existing sand bar.

Sand bars on natural beaches typically move slowly shoreward when wave energy is low, and move more rapidly offshore when waves are energetic and the wave-driven circulation is strong (Winant et al. 1975, Aubrey 1979, Jaffe et al, 1984, Wright and Short 1984, Lippmann and Holman 1990, and others). Although the net direction of bar motion is known from pre- and post-storm bathymetric surveys, continuous observations of the bathymetric evolution of a natural beach during high-energy waves have only recently been obtained (using downward-looking sonar altimeters mounted on fixed frames, Gallagher et al. 1996). Here, about 2 months of nearly-continuous observations with 9 altimeters (and colocated current meters) are used to describe and model bar-dominated bathymetric evolution along a cross-shore transect extending from about 1- to 4-m water depth.

Models for the evolution of the cross-shore profile (including sand bars) include equilibrium profile (Bruun 1954, Dean 1977), descriptive (Wright and Short 1984, Lippmann and Holman 1990), empirical profile evolution (Kriebel and Dean 1985, Kraus and Larson 1988), and process-based models (Bowen 1980, Bailard 1982, Dally and Dean 1984, Watanabe and Dibajnia 1988, Roelvink and Stive 1989, Thornton et al. 1996). Roelvink and Brøker (1993) review profile evolution models. Process-based models attempt to account explicitly for the physical processes

effecting bathymetric evolution. Process-based energetics-type sediment transport models (based on Bagnold 1966, described in section 3 below) relate sediment transport to the near-bottom flow field and are frequently used to predict morphological evolution. Bowen (1980) used this type of transport model with simplified flows to describe nearshore sediment motions, and demonstrated improved predictions of beach slope and sediment size distribution across the beach relative to the null-point model (Eagleson and Dean 1961). Bailard (1982) also assumed simple wave-driven flows and predicted beach volume change. Improved predictions of profile changes using the energetics transport model are reported to result from including (in the wave and wave-driven circulation models) undertow (Stive and Battjes 1984), wave asymmetry (Stive 1986, Nairn and Southgate 1993), breaking-induced turbulence (Roelvink and Stive 1989), and infragravity waves (Sato and Mitsunobu 1991). Roelvink and Stive (1989) compared cross-shore profile evolution observed in the laboratory with predictions of an energetics-type model. The near-bottom flows (predicted with a different model) driving the sediment transport included all of the above processes. Roelvink and Stive (1989) concluded that the vertically integrated, quasi-steady response assumed in the energetics transport model was of limited validity in the nearshore. However, performance of the sediment transport model is difficult to evaluate in studies where the predicted transport also depends on the accuracy of the hydrodynamic models.

Dally and Dean (1984), Sallenger and Howd (1989), and many others have suggested that bar formation and/or migration is caused by offshore directed, near-bottom, wave-driven, steady flows ("undertow"). However, undertow is not well understood even on planar beaches where the wave transformation is well parameterized (eg, Stive and Wind 1986, Svendsen and Buhr Hansen 1988, Masselink and Black 1995). On barred beaches wave transformation is more complex because wave-breaking is enhanced near the bar crest and reduced in the bar trough (Lippmann et al. 1996). Bar-intensified undertow has been observed previously (Sallenger and Howd 1989, Smith et al. 1992, and Haines and Sallenger

1994). Thornton et al. (1996) used near-bottom velocities observed for 10 days on a densely instrumented cross-shore transect at Duck, NC to drive an energetics transport model. The morphology was usually measured daily with the CRAB (a large amphibious vehicle), but there were up to 48 hrs between some surveys because the CRAB cannot operate when the significant wave height H_s exceeds about 2 m (Lee and Birkemeier 1993). The model predicted the offshore migration of the sand bar observed during high-energy waves and strong mean flows, but not the slight onshore bar motion and other small profile changes observed during low-energy conditions.

The present study supports and extends the results of Thornton et al. (1996). Currents observed on the same Duck, NC beach (the observations are described in Section 2) are used to drive the same energetics sediment transport model (described in Section 3). The nearly continuous observations of the currents and cross-shore profile allow comparison of measured and predicted beach profiles during storms, as well as between them. Observed and modeled changes in the beach profile are compared (Section 4) for 4 several-day long events, and for a continuous 60 day period. Offshore bar migration during storms is predicted well. Gradients in the modeled suspended sediment transport caused by bar-intensified undertow is the dominant term contributing to offshore bar migration. Megaripples (observed with a small array of 7 altimeters in the trough shoreward of the sand bar, see Section 2) were often present, both during low and high wave conditions. Bedform-induced phase lags could contribute to poor model performance during low wave-energy conditions, when oscillatory currents are larger than steady currents. The results are summarized in Section 5.

2. Observations

The data were obtained during the Duck94 field experiment conducted near Duck, NC on a barrier island exposed to the Atlantic ocean. Colocated sonar altimeters, pressure sensors, and bidirectional Marsh-McBirney electromagnetic

current meters, sampled at 2 Hz, were deployed on fixed frames at 9 locations on a 255-m long cross-shore transect. Colocated pressure and current meters (but no altimeter) were deployed at 4 additional locations along the transect (Figure 2.1). The average spacing between flowmeters is about 20% less than in Thornton et al. (1996). The shallowest sensors were located near the toe of the steep foreshore, so the swash zone was not instrumented. The seafloor location directly under each altimeter (averaged over the approximately 6-cm diameter circular footprint) was estimated from the altimeter data using algorithms described in Gallagher et al. (1996). Temporal averaging of the seafloor location estimates ranges from 32 s to 24 hr. The altimeter-based cross-shore profiles are spatially sparse, but still resolve features observed in spatially dense (but infrequent) CRAB profiles (Figure 2.1).

Between 15 Aug and 26 Oct the sand bar moved 130 m offshore with 1.5 m of erosion near the initial location of the bar crest and 1 m of accretion at the final offshore bar location (Figure 2.1). Most of the offshore migration (Figures 2.2a and b) occurred during high-energy wave conditions ($H_s > 2$ m, Figure 2.2d). Slight onshore bar movement occurred during periods of low waves. Offshore bar migration rates, based on the location of the bar crest estimated from successive 3-hr profiles, were larger than the onshore migration rates (Figure 2.2b). The estimates of bar crest position and migration speed (especially the low speeds associated with slight onshore bar motion) are only qualitative owing to the relatively large spatial separation between altimeters. CRAB profiles (when available) were used to improve the estimated bar crest locations.

With Δ_n the measured change in seafloor elevation at each of the N sensors along the cross-shore transect, the cross-shore mean and root-mean-square (RMS) changes are

$$\Delta_{\text{net}} = \frac{1}{N}\sum_{n=1}^{N} S_n \Delta_n \qquad (1a)$$

and

$$\Delta_{\mathrm{RMS}} = \sqrt{\frac{1}{N}\sum_{n=1}^{N}(S_n\Delta_n)^2} \qquad (1b)$$

The observed changes are weighted by $S_n = \frac{\frac{1}{2}(dx_{n-1}+dx_n)}{\bar{dx}}$ where $dx_n = x_{n+1} - x_n$ is the separation between adjacent sensors and $\bar{dx}$ is the average sensor separation. Time series of Δ_{net} and Δ_{RMS} based on successive 24 hr-average profiles are shown in Figure 2.2c. The mean change (Δ_{net}) is equal to the thickness of the sediment layer apparently lost (or gained) daily along the cross-shore array, and Δ_{RMS} is the typical magnitude of daily changes in the seafloor location. If sand is conserved (eg, no longshore transport divergence and no transport from within the array to locations shoreward or seaward of the array) and the profile is spatially sampled adequately, then $\Delta_{\mathrm{net}} = 0$. The observed daily Δ_{net} of ± 5 cm is small compared to the $\Delta_{\mathrm{RMS}} = 10 - 20$ cm observed during bar motion events (Figure 2.2c). The mean and RMS changes (1) were also calculated using profile changes Δ_n based on 3-hr average profiles from the beginning and end of events (Table 2.1). For the several-day bar motion events studied in detail ('a' – 'd' in Figure 2.2c, Table 2.1) and for the 2-month long modeled period (1 Sep – 28 Oct, Table 2.1) the observed Δ_{net} is small compared with Δ_{RMS}. Thus, observed changes in the profile when the bar moves can be largely accounted for by redistribution of sediment within the measured profile.

The largest changes in successive daily profiles (eg, peaks in the daily Δ_{RMS}, Figure 2.2c) and the most rapid changes in bar location (Figure 2.2b) are correlated with both offshore significant wave height (Figure 2.2d) and the magnitude of mean and oscillatory currents near the bar crest (Figure 2.2e). When the observed cross-shore mean current was greater than about 40 cm/s, the maximum cross-shore mean current occurred just shoreward of the bar crest (Figure 2.3a). Although the cross-shore location of the maximum mean longshore current was more broadly distributed, the maximum was often located close to the bar crest (Figure 2.3b). These strong mean currents contribute significantly to the bar

motion predicted by the sediment transport model.

The four cross-shore transport events investigated in detail include 3 examples of offshore bar motion during relatively high-energy conditions (labeled 'a', 'c', and 'd' in Figure 2.2c) and one case ('b' in Figure 2.2c) of onshore bar motion. Event 'd' (10 - 15 Oct, Figure 2.2) includes a portion of the period with the largest observed profile change (10 - 20 Oct, Figure 2.4) and the largest observed H_s (4 m). During this nor'easter storm, approximately 1.5 m of erosion occurred at the original location of the bar (x=240 m, Figure 2.4) and 0.9 m of accretion 80 m offshore (x=320 m, Figure 2.4). The sand bar migrated steadily offshore and the profile evolved gradually (Figures 2.2b and 2.4), in contrast to suddenly or catastrophically as might occur if the sand bed were fluidized (Seymour 1986). The sand bar migrated about 50 and 20 m offshore during events 'a' and 'c' (Figures 2.5a and c, respectively), and migrated onshore about 20 m during event 'b' (Figure 2.5b).

Time series of seafloor location measured with a two-dimensional 1.4 X 1.4 m coherent array of 7 altimeters located in the trough of the sand bar ($x = 170$ m) suggest migrating megaripples (Hay and Wilson 1994) with heights of O(20 cm) were often present. Numerous visual observations confirmed the presence of megaripples with wavelengths of a few meters. Megaripple migration speeds were estimated from the sensor separations and the corresponding time lags to the maximum of the cross correlations between time series for each sensor pair on the cross- or longshore axes of the array. Average resultant speed and direction were calculated from the cross- and longshore components. Changes in megaripple migration direction are not accounted for in this analysis.

Migration speeds and directions of megaripples during each of the 4 bar-moving events ('a'-'d') discussed above were estimated from the array data. Between 2 and 3 Sep (during event 'a'), megaripples (Figure 2.6a) migrated 100 cm/hr toward the south, approximately aligned with the mean current vector (46 cm/s, Figure 2.7a). Between 26 and 27 Sep (event 'b'), megaripples (Figure 2.6b)

migrated onshore at 34 cm/hr, whereas the mean current vector (27 cm/s) pointed northeast (Figure 2.7b). Megaripples in event 'c' migrated toward shore, but the mean current vector (27 cm/s) was alongshore (Figure 2.7c). Mean currents between 11 and 15 Oct changed from southeasterly (17 cm/s) to offshore (9 cm/s) to northeasterly (18 cm/s), but the megaripple migration direction, although possibly influenced by the mean current direction, was predominantly onshore (Figures 2.7d, e, and f).

Nearshore megaripples are often assumed to be dominated by steady flows, similar to dunes (Middleton and Southard 1984, Nielsen 1992, Fredsøe and Diegaard 1992). Raudkivi (1990) suggests that waves lower the threshold of sediment motion, allowing small steady currents to move megaripples. However, only one of the 6 megaripple migration directions was within 45° of the mean current direction (Figure 2.7a). Hay and Wilson (1994) also observed onshore megaripple migration under similar flow conditions (mean current $\approx$ 15 cm/s, parallel to shore) on the crest of a sand bar in Lake Huron during the waning stages of a storm. Clifton (1976) suggested onshore megaripple migration in the nearshore resulted from skewed oscillatory velocities (eg, the onshore flow is stronger and of shorter duration than the offshore flow). Skewness contributes to transport in energetics-based models (Bailard 1981). The skewed oscillatory flow is represented by the RMS oscillatory cross-shore and longshore flows $\langle\tilde{u}^2\rangle^{1/2}, \langle\tilde{v}^2\rangle^{1/2}$ weighted by the respective velocity skewness $\langle\tilde{u}^3\rangle/\langle\tilde{u}^2\rangle^{3/2}, \langle\tilde{v}^3\rangle/\langle\tilde{v}^2\rangle^{3/2}$. In 5 of the 6 cases (Figures 2.7b–f), megaripple migration was within 40° (4 of 6 within 20°) of the direction of these skewness-weighted orbital velocities.

The altimeter accuracy is about 2-3 cm (Gallagher et al. 1996). However, 3-hr average estimates of the mean seafloor location (eg, Figures 2.4 and 2.5) can contain errors of O(10 cm) owing to slowly migrating megaripples beneath the altimeters (shown in Figure 2.6). A longer averaging time would reduce errors by including more of the megaripple profile in the average, but would degrade the temporal resolution of the estimated profile changes.

Hydraulic flow drag over bedforms is larger than over a smooth bed, and bedforms thus affect friction factors used in nearshore circulation and sediment transport models (Nielsen 1992). A roughness for each 3-hr period for each altimeter on the transect was crudely estimated by assuming that RMS fluctuations in linearly detrended (over 30 hrs to remove contributions from larger-scale erosion or accretion) seafloor location time series result from bedforms migrating under the altimeters. The example altimeter time series (Figure 2.6) have roughness of about 7 - 8 cm. RMS fluctuations ranged from 0 to 10 cm and are not correlated with significant wave height. The estimated roughness decreased significantly in amplitude offshore of the bar (Figure 2.8).

3. Model

Assuming the energy dissipation of a unidirectional stream occurs via shear stress at the bed and that a fraction of the dissipated energy (or power) is used to move sediment, the total sediment transport rate i is (Bagnold 1966)

$$i = i_b + i_s = \left(\frac{\epsilon_b}{tan\phi - tan\beta} + \frac{\epsilon_s(1-\epsilon_b)}{(W/\overline{u}) - tan\beta}\right)\omega \qquad (2)$$

where subscripts b and s refer to bedload and suspended load, β is the bed slope, ϕ is the angle of internal friction (angle of repose), and W is the sand grain fall velocity. The dissipated stream energy ω, equal to the product of the assumed quadratic shear stress at the bed ($\tau = \rho_w C_f |\overline{u}|\overline{u}$) and the mean free stream velocity $\overline{u}$, is

$$\omega = \tau\overline{u} = \rho_w C_f |\overline{u}|^3$$

where ρ_w is the water density and C_f is a friction coefficient. The efficiency factors ϵ_b and ϵ_s are the percent of power used for bedload and suspended load. Above a critical value of ω, Bagnold (1966) argued that $0.11 \leq \epsilon_b \leq 0.14$ and $\epsilon_s = 0.01$.

Bailard (1981) and Bailard and Inman (1981) extended the steady-flow

transport equation (2) to combined unsteady (eg, oscillatory) and steady flows. Assuming the beach slope is small, the resulting time-averaged, cross-shore volume sediment transport per unit width per unit time is (Bailard 1981)

$$Q_x = K_b\{\langle|\vec{u}|^2\tilde{u}\rangle+\langle|\vec{u}|^2\overline{u}\rangle-\frac{tan\beta}{tan\phi}\langle|\vec{u}|^3\rangle\}+K_s\{\langle|\vec{u}|^3\tilde{u}\rangle+\langle|\vec{u}|^3\overline{u}\rangle-\frac{\epsilon_s}{W}tan\beta\langle|\vec{u}|^5\rangle\} \quad (3)$$

where $\vec{u}$ is the total (ie, cross- and longshore) near-bottom velocity vector, $\overline{u}$ and $\tilde{u}$ are the mean and oscillatory components of the cross-shore near-bottom velocity, respectively, $\tan\beta$ is the local cross-shore beach slope, and $\langle\ \rangle$ indicates time average. The coefficients K_b and K_s are

$$K_b = \frac{\rho_w}{\rho_s-\rho_w}C_f\frac{\epsilon_b}{\tan\phi};\quad K_s = \frac{\rho_w}{\rho_s-\rho_w}C_f\frac{\epsilon_s}{W}$$

and ρ_s is the sand density.

Cross-shore sediment transport Q_x depends on longshore, as well as cross-shore, currents because both contribute to the total stress that mobilizes sediment. Based on comparisons of model predictions using offshore wave and current conditions with measured beach change, Bailard (1982) suggested that $\epsilon_b = 0.13$ and $\epsilon_s = 0.01$, similar to the results of Bagnold (1966), although the 95% confidence interval of these estimates was large. Following Thornton et al. (1996), here $\epsilon_b = 0.135$, $\epsilon_s = 0.015$, and $C_f = 0.003$ (Church and Thornton 1993). The present model predictions are not sensitive to ± 30 % changes in these parameters, nor to removing a few flowmeters, nor to plausible errors in the measured currents, as discussed in the appendix.

Assuming there are no gradients in longshore sediment flux and the density of sediment packing is constant, mass conservation in the cross-shore direction yields

$$\frac{dQ_x}{dx} = \mu\frac{dh}{dt} \quad (4)$$

where h is bed elevation and μ is a packing factor ($\mu = 0.7$ is used here, Thornton et al. 1996).

Thornton et al. (1996) predicted profile change at Duck, NC (Oct 1990) with this model initialized with CRAB profiles and driven by observed currents. Similarly, here the transport model is initialized with 3-hr altimeter profiles and driven with observed currents. The model bed-elevation change between adjacent current meters is calculated using a finite-difference scheme and then interpolated to approximate elevation change at the locations of the altimeters.

4. Model-Data Comparisons

The model performance is expressed as the predictive skill, defined here as $1 - \frac{P_{\mathrm{RMS}}}{\Delta_{\mathrm{RMS}}}$ where P_{RMS} is the RMS prediction error (ie, the RMS difference between predicted and observed final 3-hr averaged profiles) and Δ_{RMS} is the RMS change between the initial and final observed profiles (1b). (Both P and Δ are weighted by the sensor separation.) If the errors vanish, then skill = 1. The skill = 0 if the errors are as large as the observed changes, in which case the model prediction is not better than a prediction that the final profile equals the initial profile. The skill is negative if errors in the prediction are larger than the observed changes. The initial and final profiles that bracket periods of low wave energy can be similar (eg, Δ_{RMS} is small), resulting in low skill (Table 2.1) even though the absolute errors in the predictions are not large.

Using the same parameters as Thornton et al. (1996) (with the exception of fall velocities, discussed below), the model predicts accurately the overall profile changes and the offshore migration of the sand bar observed during a large nor'easter storm (event 'd', 10–15 Oct 1994, $H_s > 2$ m) (Figure 2.9). Although the conditions near the sand bar ($\overline{u}_{max} = 60$ cm/s, $\overline{v}_{max} = 100$ cm/s) were similar to those in 1990 ($\overline{u}_{max} = 50$ cm/s, $\overline{v}_{max} = 125$ cm/s) observed by Thornton et al. (1996), the model has much higher skill for the 1994 data. Thornton et al. (1996) underpredict the observed erosion in the trough, whereas both erosion and

accretion are predicted well here (Figure 2.9). Thornton et al. (1996) used the same value of the fall velocity ($W = 1.3$ cm/s) for all cross-shore locations except the shallowest, whereas here a variable W ($1.3-3.5$ cm/s) is used. The cross-shore distribution of fall velocity was estimated (following Sleath 1984) from sediment size measured along the transect (Stauble 1992, Stauble pers. comm. 1995). The model skill for the 5-day period shown in Figure 2.9a is 0.66 for spatially varying W and 0.39 for constant W (Table 2.1). The skill is 0.14 for the constant W prediction shown for a 7 day event in Figure 11 in Thornton et al. (1996). Spatially variable W results in higher skill for all predictions discussed here (Table 2.1).

The offshore migration of the sand bar observed in event 'a' ($H_s = 2.8$ m and maximum offshore-directed currents $\approx$ 60 cm/s) is predicted accurately (Figure 2.10a, skill=0.48). Comparison of observations and predictions every 3 hrs (Figure 2.11a) shows some deviation as the bar moves past the sensor at x=220 m (3 Sep 1200 - 4 Sep 1200 hrs), but the final prediction is accurate. The small profile changes predicted for event 'c' are considerably less than observed (Figures 2.10c and 2.11c, skill=0.28). In this case, high waves ($H_s = 2.5$ m) occurred for a relatively short period and the maximum offshore-directed current was relatively low ($\approx$ 30 cm/s, Figure 2.2). The model has no skill in predicting the approximately 20 m onshore bar movement observed in event 'b' (Figure 2.10b, skill = 0.02). Between 22 and 27 Sep there are small ($\pm$5 cm) predicted changes (onshore accretion, offshore erosion) before the final prediction of no change (Figure 2.11b).

The cross-shore bathymetric evolution was predicted over the entire 2-month data set by initializing with the profile observed on 1 Sep and driving with currents observed every 3-hr period until 28 Oct. As shown in Figure 2.12a, model skill is high ($\approx$ 0.5) for the first 20 days and then decreases to $\approx$ 0 between 20 Sep and 2 Oct, which includes event 'b' and the period of greatest onshore bar migration (Figure 2.2b). On 2 Oct, the bar crest is about midway between the initial and predicted locations (Figure 2.12c). The skill generally increases when the bar moves offshore. Sixty days after initialization, the predicted and observed

profiles are similar (skill = 0.44, Figure 2.13). The predicted maximum offshore migration rates of the sand bar (Figure 2.12d) (based on the predicted location of the bar crest, Figure 2.12c) are about half of the observed rates. Onshore migration was not predicted. Predictions and observations of 3-hr averaged seafloor change at four cross-shore locations for the entire 2 month period are shown in Figure 2.14. At some locations the model predicts elevation change when it was observed (eg, Figures 2.14c and d), but errors can increase at locations where onshore bar migration is poorly modeled (eg, 22 – 27 Sep at x=220 m, Figure 2.14b).

To investigate the conditions under which the model succeeds or fails the terms of the total sediment transport Q_x are examined separately. The first three terms on the right hand side of (3) represent bedload transport and the second three correspond to suspended load. The three terms of each group represent transport driven by asymmetries in the oscillatory flow $\tilde{u}$, by the mean flow $\overline{u}$, and by gravity, respectively. Previous model studies (Stive 1986, Thornton et al. 1996, and others) suggest that the gravity-driven and bedload transport terms are relatively small on a natural beach, as is the case here. Suspended load driven by oscillatory and mean currents dominates the predicted total transport Q_x in all cases, as shown for intense storm conditions (11 Oct, event 'd') in Figure 2.15a.

Changes in the profile result from gradients in the total transport dQ_x/dx (4). During storm event 'd', dQ_x/dx is dominated by gradients in the mean-flow-driven transport that result in erosion on the shoreward side of the bar crest and accretion offshore (solid circles in Figure 2.15b). Other modeled gradient terms are relatively small, except for gradients of the oscillatory-flow-driven suspended transport that results in accretion near the bar crest (open circle at $x = 250$ m in Figure 2.15b). In storm event 'a', gradients of mean- and oscillatory-flow-driven suspended transport contribute roughly equally to dQ_x/dx over much of the profile (Figure 2.16a). The predicted gradients in total transport are similar to observed values in these two storms (compare dashed and solid lines in Figures 2.15b and 16a). Although the modeled total transport gradient is underpredicted for storm

'c', the trend (erosion in the trough and accretion offshore) is reproduced (compare dashed and solid lines in Figure 2.16c). In all 3 storms, measured offshore-directed mean flows were maximum just shoreward of the bar crest, and gradients in these flows tend to move the bar offshore. The model predicts no significant profile change when wave energy was low and steady flows were weak (event 'b', Figure 2.16b). Onshore bar migration was observed in this case.

The energetics transport model was developed for unidirectional river flows (Bagnold 1966). The model for combined mean and oscillatory flow (3) is based on the assumption that sediment suspension occurs instantaneously in response to fluid forcing, so that the fluid velocity, sediment suspension, and transport are all in phase. However, sediment suspended at one phase of the wave is in fact transported during subsequent phases before settling to the bed (Hanes and Huntley 1986 and many others). Sediment-laden vortices in the wake of ripples or megaripples may alter the amount of suspended sediment relative to that above a flat bed and may also enhance the phase lag between suspension and transport (Inman and Bowen 1963). Additionally, sediment transport in oscillatory flow may depend on fluid accelerations (not accounted for in the present model), as well as velocities (Hallermeier 1982, Hanes and Huntley 1986, and others). The energetics model is therefore expected to perform best for flows dominated by quasi-steady currents with sheet flow conditions over a smooth bed (Roelvink and Stive 1989).

The 60 days of data were subdivided into 5 periods with significant profile evolution and 5 periods of little or no change (dates are given in Table 2.1 and Figure 2.17). As discussed above (eg, Figure 2.6) megaripples were often present. However, model skill is not significantly correlated with average (across the transect) RMS bed roughness (r=0.27). Model skill is correlated with the ratio of the maximum (near the bar crest) average (over the modeled period) mean velocity to the maximum average root mean square velocity

$$\frac{\langle(\overline{u}^2+\overline{v}^2)^{1/2}\rangle}{\langle(\langle\tilde{u}^2\rangle+\langle\tilde{v}^2\rangle)^{1/2}\rangle}$$

(r=0.71, significant at the 95% level). The model skill is highest during the 4 periods when mean currents are dominant and the profile changes significantly (open symbols with skill > 0.25 in Figure 2.17). Model skill is low for the 6 periods when the oscillatory flow is dominant and there is either relatively little profile evolution (filled symbols) or onshore bar migration (open diamond). Perhaps phase lags between between suspension and transport over the megaripples increase in importance as oscillatory currents increase relative to mean flows. There are numerous other possible sources of model error. For example, vertical shear in the mean cross-shore current may be significant, but the observed mean is used directly in the transport equation (3). Gradients in the alongshore sediment transport are neglected in the profile change model (4), but the bathymetry was sometimes highly irregular in the alongshore direction. The beach change model is based on limited understanding of both sediment and hydrodynamic processes, but does parameterize the dependence of sediment transport gradients (which cause morphology change) on the flow.

5. Summary

Nearshore morphology and currents were measured nearly continuously for two months at Duck, NC. Newly developed sonar altimeters were used to estimate the location of the seafloor along a cross-shore transect, even during storms when traditional surveying techniques fail. The sand bar moved approximately 130 m offshore, at rates O(60 cm/hr), primarily during three periods with energetic waves (offshore significant wave heights > 2 m). Slight onshore bar migration was observed under small waves.

Megaripples (bedforms) with amplitudes $\approx$ 20 cm were observed to migrate at speeds from 30 to 100 cm/hr under a small array of altimeters located in the trough of the sand bar. The megaripples usually migrated onshore, nearly aligned with the skewed oscillatory velocity vector.

An energetics-based sediment transport model predicts accurately the

seaward bar motion observed when waves are energetic and near-bottom offshore directed mean currents (eg, undertow) are strong. The dynamics of breaking waves on sand bars are only qualitatively understood, but bar-intensified breaking causes a maximum in the undertow just shoreward of the bar crest, and the predicted offshore bar migration is driven by corresponding gradients in the modeled suspended sediment transport. When the wave energy decreases, wave breaking on the bar is reduced and both the observed and predicted bar migration rates decrease. Although the bar sometimes moved slowly onshore during periods of low waves, whereas little or no profile change is predicted, these changes are small relative to the well-modeled offshore bar movements during storms. Thus, even though the energetics model was developed for unidirectional flow over smooth riverbeds and may be inaccurate for oscillatory-dominated flows over ripples and megaripples, the model predicts qualitatively the cross-shore bar migration and profile evolution observed over a 2-month period on a natural beach.

6. Appendix: Model Sensitivity

Model skill was calculated for the large offshore bar migration observed 10 - 15 Oct (event 'd') for $0.005 \leq \epsilon_s \leq 0.04$ (with fixed ϵ_b and C_f) and $0.002 \leq \epsilon_b \leq 0.50$ (with fixed ϵ_s and C_f). The highest skills are for $\epsilon_s = 0.015$ and $\epsilon_b = 0.135$ (Table 2.2). The sensitivity to ϵ_s is much greater than to ϵ_b, consistent with the dominance of suspended load compared with bed load transport (Figure 2.15). The skill is not sensitive to variation of ϵ_s over the range 0.01 - 0.02.

Church and Thornton (1993) suggest $0.001 \leq C_f \leq 0.006$. Although model skill (with fixed ϵ_s and ϵ_b) is not greatly effected for $0.002 \leq C_f \leq 0.004$, C_f values outside this range result in significantly decreased skill (Table 2.2).

The model predictions also are not sensitive to plausible measurement errors. For each of 100 simulations of event 'd', a random offset uniformly distributed between ± 6 cm/s offset was applied to each current meter for the duration of the event (representing a quasi-stable offset error with magnitude roughly representa-

tive of the errors in these observations). The simulations produced a mean model skill of 0.5 with a relatively small standard deviation of 0.1. Likely errors in the orientations of the current meters ($\pm 5°$) resulted in a mean model skill of 0.65, with standard deviation of 0.02. The model skill for event 'd' also varied by less than 10% when a few arbitrarily selected sensors were excluded from the model-data comparisons.

Table 2.1: Δ_{net} (cm), Δ_{RMS} (cm) (based on 3-hr profiles at the beginning and end of the indicated time periods), and model skill (using constant or variable fall velocity W) for short periods (determined by amount of beach change and sensor availability) and for the entire 60-day period. The periods labeled (a) - (d) are discussed in detail.

Beach Change						
	1–5 Sep (a)	9–22 Sep	22–27 Sep (b)	28 Sep – 2 Oct	2–4 Oct (c)	5–10 Oct
Δ_{net}	3.1	-6.1	1.4	0.0	-3.8	-4.5
Δ_{RMS}	40.2	9.7	19.8	5.2	19.7	7.5
Model Skill						
constant W	0.30	-1.98	0.02	-0.27	0.23	-1.78
variable W	0.48	-0.75	0.02	-0.12	0.28	-0.70

Beach Change: con't					
	10–15 Oct (d)	16–20 Oct	21–25 Oct	26–28 Oct	1 Sep – 28 Oct
Δ_{net}	-13.3	9.5	7.7	7.4	7.2
Δ_{RMS}	65.6	40.1	16.9	11.7	84.2
Model Skill: con't					
constant W	0.39	-0.19	-0.09	-0.20	–
variable W	0.66	0.30	-0.03	-0.02	0.44

Table 2.2: Model skill (section 4) for event 'd' (10 Oct – 15 Oct) using a range of values for ϵ_s and ϵ_b from Bailard (1982) and a range of values for C_f from Church and Thornton (1993).

Model Skills: 10 Oct – 15 Oct, event 'd'			
	$\epsilon_s = 0.015$ $\epsilon_b = 0.135$	$C_f = 0.003$ $\epsilon_b = 0.135$	$C_f = 0.003$ $\epsilon_s = 0.015$
$\epsilon_s = 0.005$		0.41	
$\epsilon_s = 0.01$		0.60	
$\epsilon_s = 0.015$		0.66	
$\epsilon_s = 0.02$		0.53	
$\epsilon_s = 0.04$		-0.35	
$\epsilon_b = 0.002$			0.65
$\epsilon_b = 0.135$			0.66
$\epsilon_b = 0.5$			0.37
$C_f = 0.001$	0.31		
$C_f = 0.002$	0.57		
$C_f = 0.003$	0.66		
$C_f = 0.004$	0.48		
$C_f = 0.006$	-0.12		

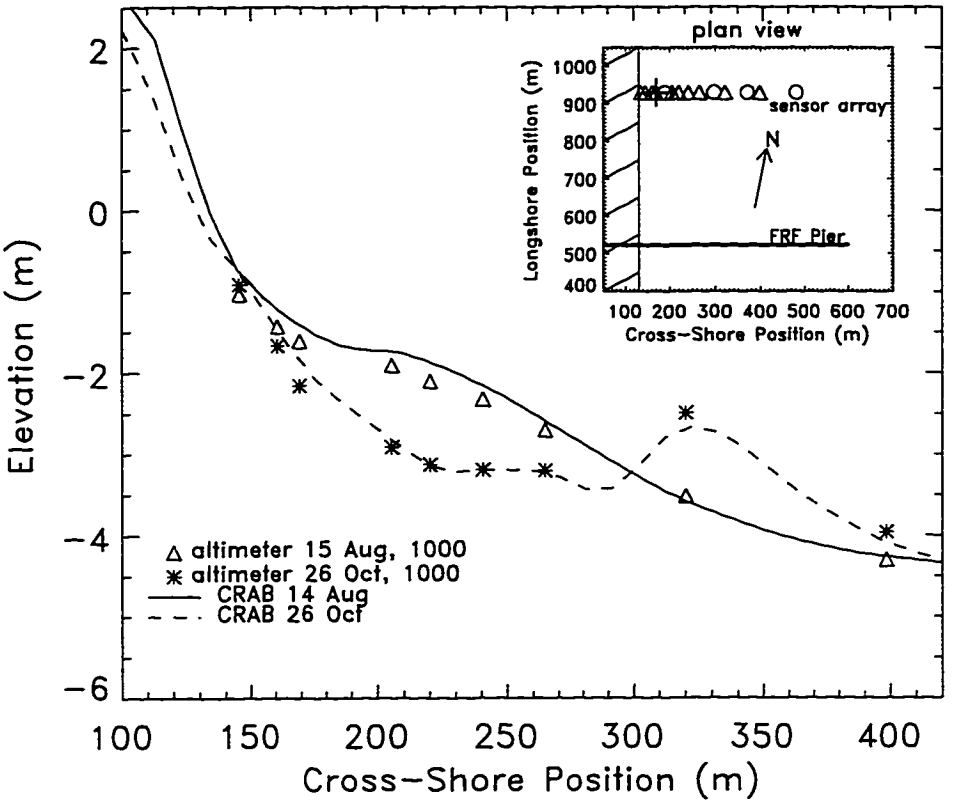

Figure 2.1: Elevation of the seafloor (relative to mean sea level) versus cross-shore position. The solid (14 Aug) and dashed (26 Oct) curves are CRAB profiles and triangles (15 Aug) and asterisks (26 Oct) are 3 hr-averaged altimeter profiles. The inset shows a plan view of instrument locations. Colocated pressure sensors, current meters, and altimeters are indicated with triangles, colocated pressure and current meters with circles, and a small coherent array of altimeters with a plus.

Figure 2.2: (a) Cross-shore location and (b) speed of migration of the sand bar crest (estimated from 3 hr-averaged altimeter profiles) versus time. (c) Net (solid curve) and RMS (dashed curve) difference between 24-hr average altimeter profiles. The periods labeled 'a', 'b', 'c', and 'd' are discussed in the text. (d) Significant wave height (3-hr average) measured in 8-m water depth and (e) currents (3-hr average) measured near the bar crest. The dotted curve is the square root of the total velocity variance, the dashed curve is the mean longshore current (positive is southward flow), and the solid curve is the mean cross-shore current (positive is onshore flow). Currents were not measured before 1 Sep, partially owing to a lightning strike that required retrieval, repair, and redeployment of many flowmeters.

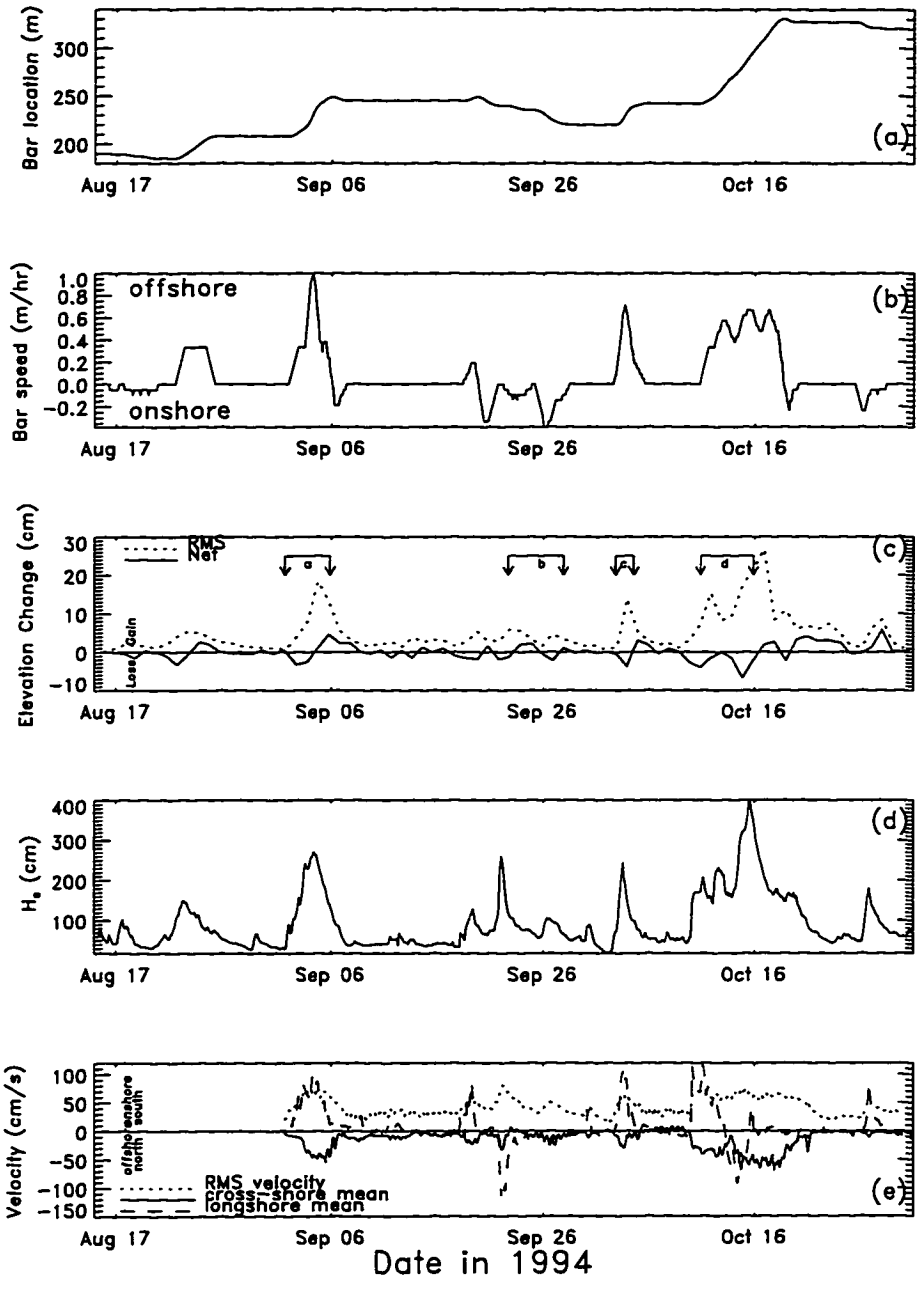

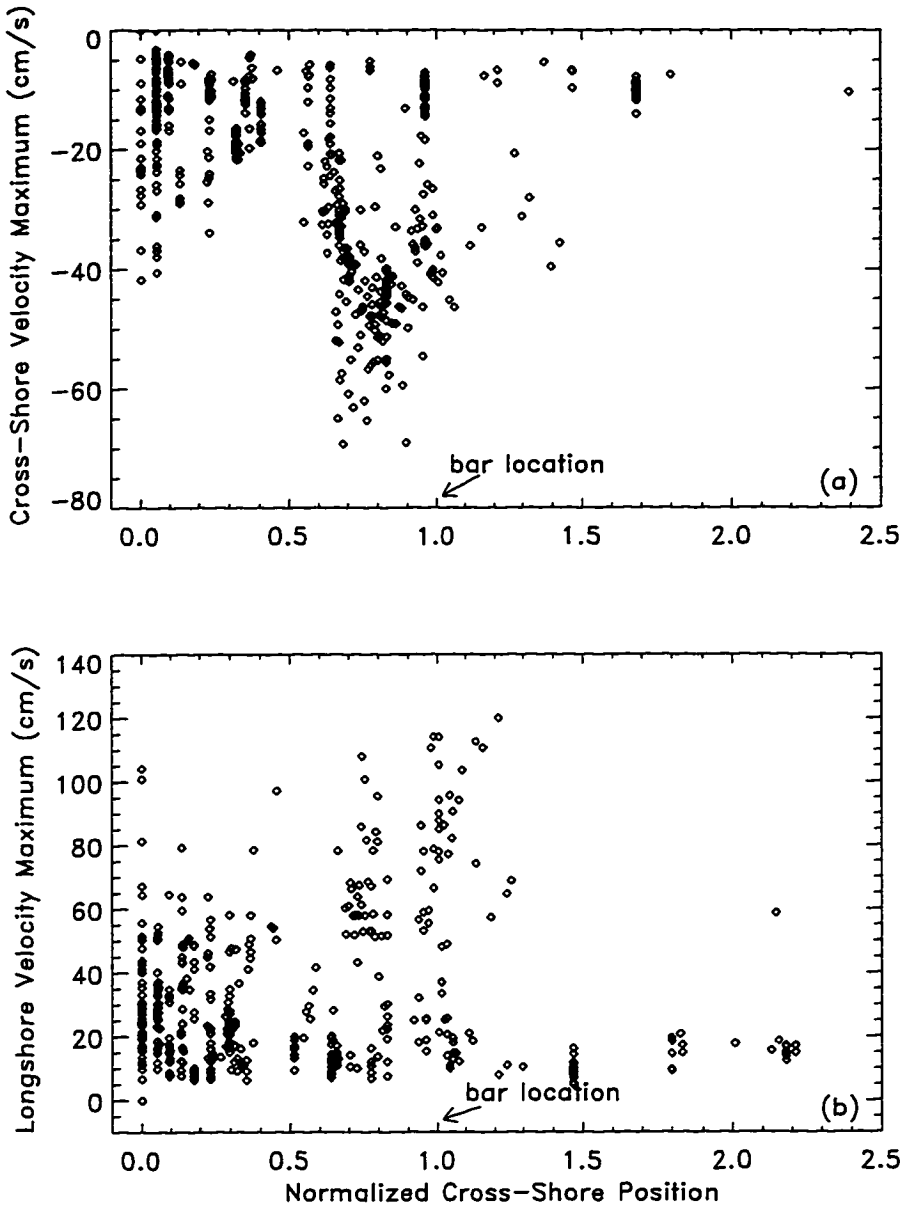

Figure 2.3: Maximum 3-hr averaged near-bottom velocity for each 3-hr period between 1 Sep and 31 Oct versus location of the maximum. Locations are normalized such that x=1 at the bar crest and x=0 at the shallowest sensor (approximately 10-20 m from the shoreline). (a) Maximum offshore-directed velocity and (b) absolute value of the maximum longshore velocity.

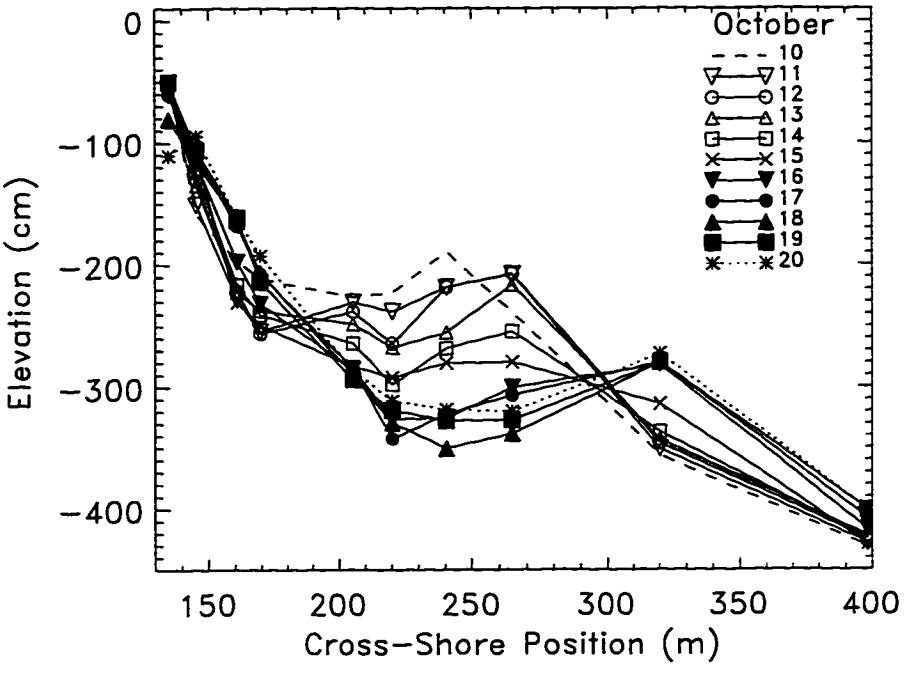

Figure 2.4: Elevation of the seafloor (relative to mean sea level) measured by sonar altimeters versus cross-shore position. One 3-hr average profile per day (2200–0100 hrs) is plotted for the 10-day storm period starting 10 Oct 2200 hrs (dates and line types are given in the legend).

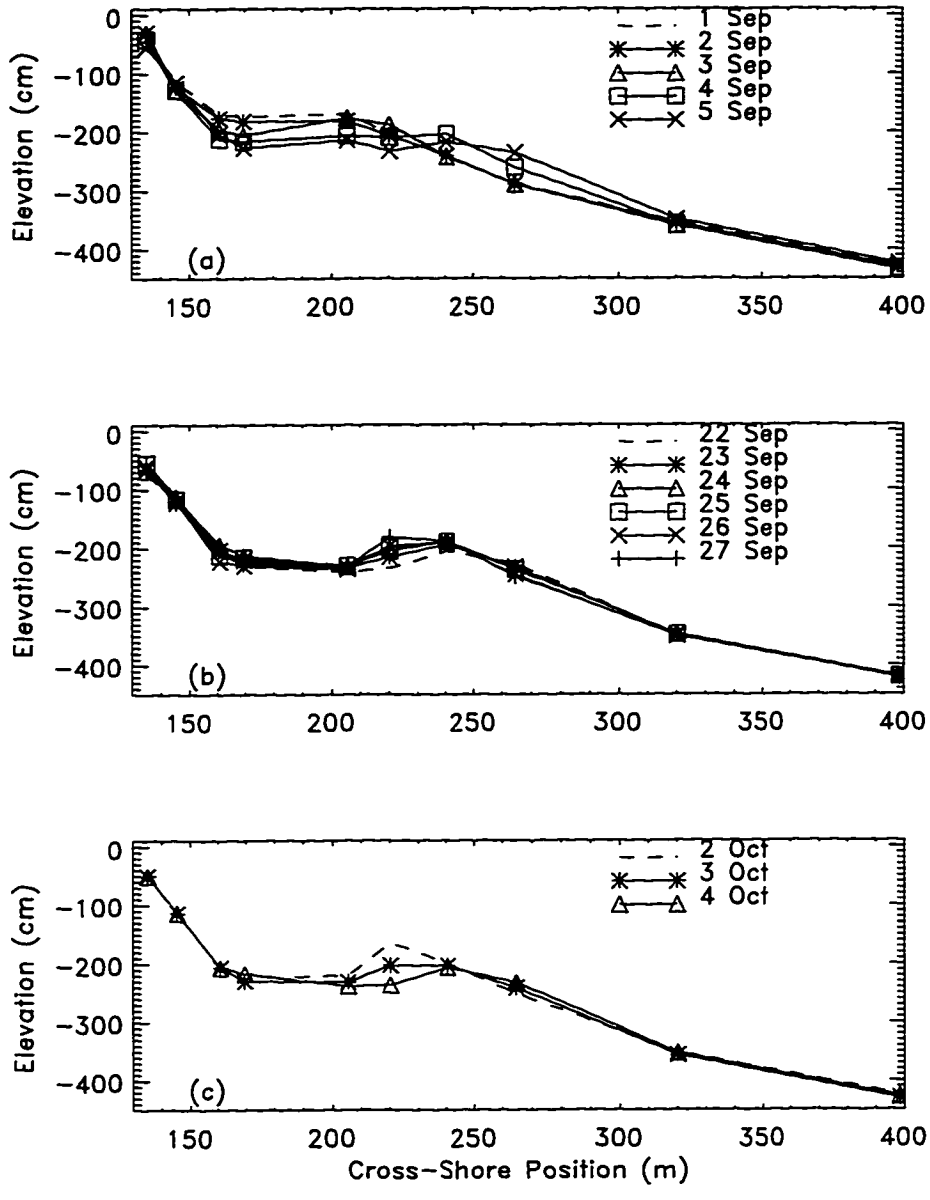

Figure 2.5: Elevation of the seafloor (relative to mean sea level) measured by sonar altimeters versus cross-shore position. One 3-hr average profile per day is plotted (dates and line types are given in legends). (a) 1–5 Sep (1900–2200 hrs), (b) 22–27 Sep (1900–2200 hrs), and (c) 2–4 Oct (1600–1900 hrs).

Figure 2.6: Distance of the seafloor below closely spaced altimeters in the 2-D array located at cross-shore location x=170 m versus time. Time series at 3 altimeters (a) along the longshore axis of the array observed between 2 Sep 0100 and 3 Sep 2200 hrs and (b) along the cross-shore axis observed between 26 Sep 0100 and 27 Sep 2200 hrs. In both cases the altimeters are separated by 80 (upper to middle panels) and 60 cm (middle to lower panels) and lines connecting the 'troughs' of the bedforms indicate migration of the features. Top panels are time series from the most northern (a) and onshore (b) altimeters.

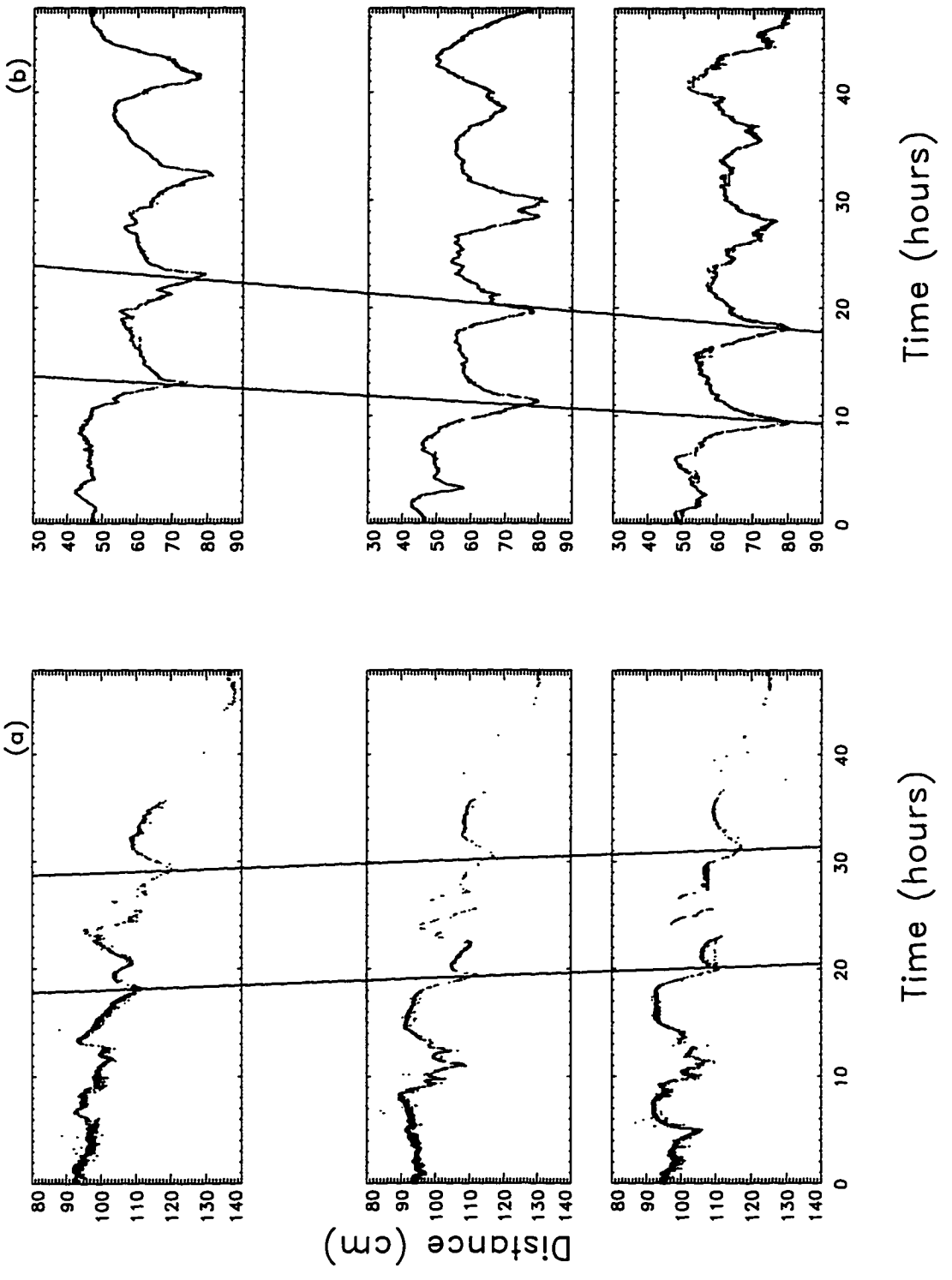

Figure 2.7: Observed megaripple migration (vector with solid filled head), mean current (vector with medium thick head), and RMS oscillatory velocity multiplied by skewness (see text, vector with thin head) for 6 events. (a) 2 Sep 0100 – 3 Sep 2200 hrs, (b) 26 Sep 0100 – 27 Sep 2200 hrs, (c) 3 Oct 0100 – 4 Oct 2200 hrs, (d)11 Oct 1600 – 13 Oct 1300 hrs, (e) 12 Oct 1900 – 14 Oct 1600 hrs, and (f) 13 Oct 1300 – 15 Oct 1000 hrs.

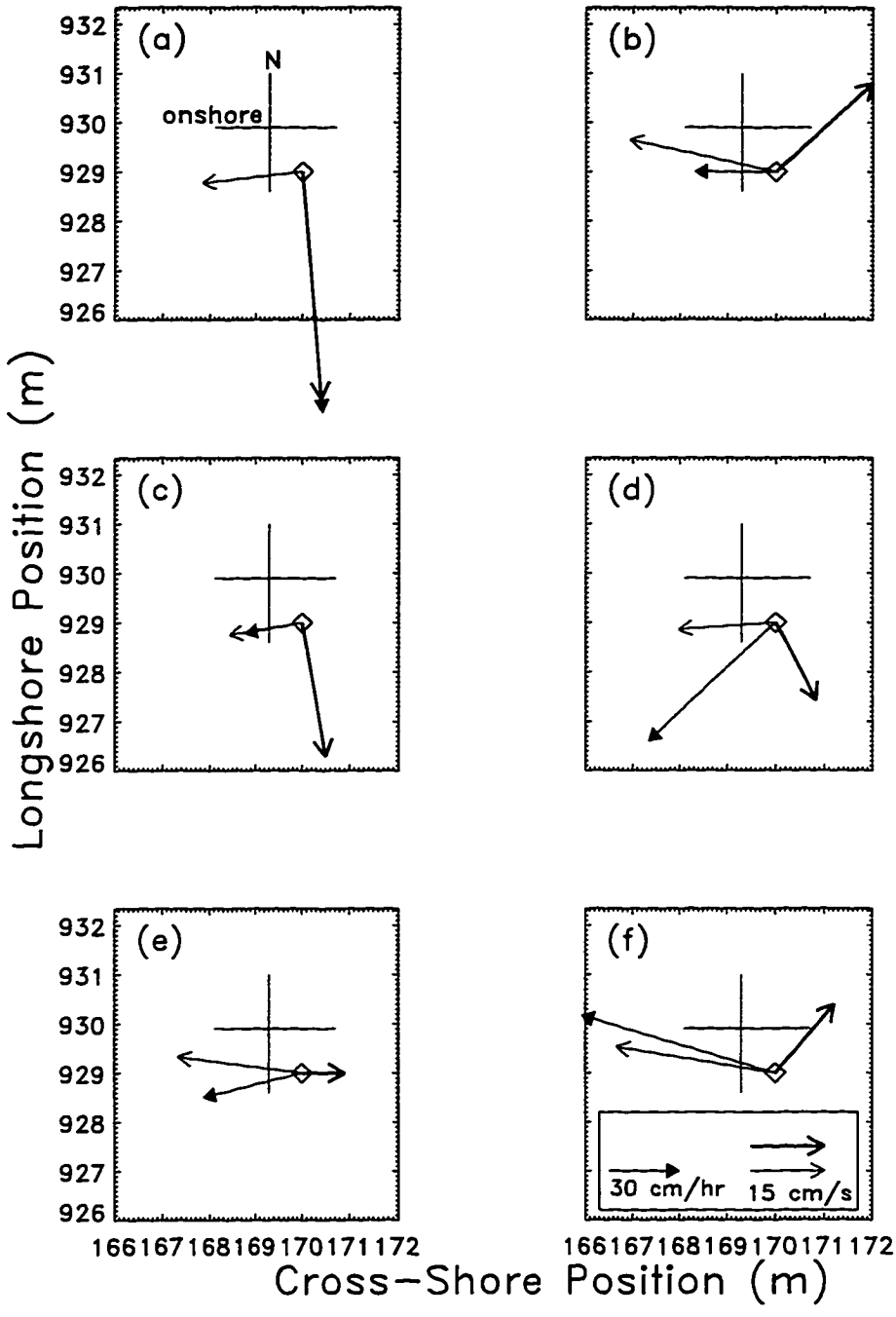

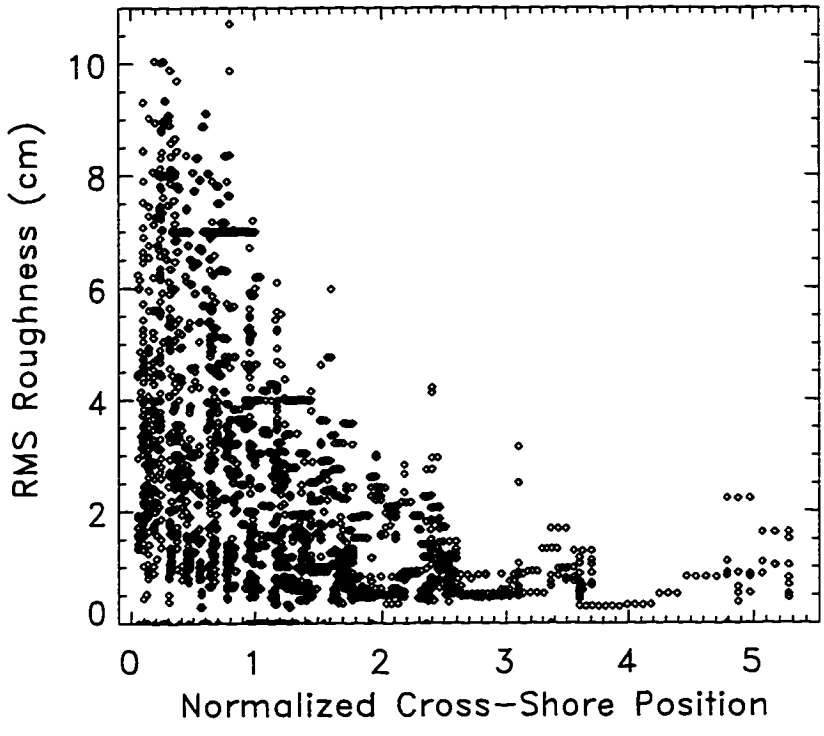

Figure 2.8: RMS roughness of the seafloor based on sonar altimeter time series for each 3-hr period between 15 Aug and 31 Oct versus cross-shore position normalized by bar crest location.

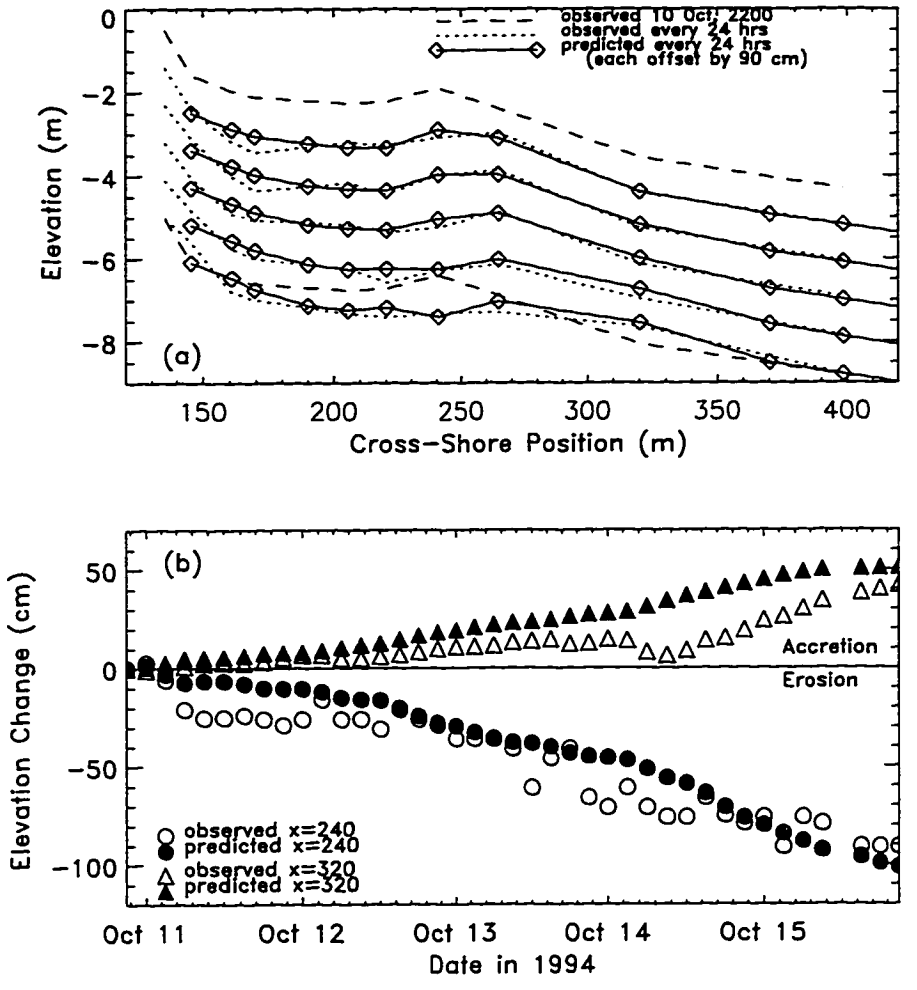

Figure 2.9: (a) Observed (dotted curves) and predicted (solid curves with diamonds) elevation of the seafloor (relative to mean sea level) versus cross-shore position. Three-hour average profiles for each 24-hour period after model initialization (10 Oct 2200 hrs, dashed curve) are sequentially offset by -90 cm in the vertical. The initial profile (dashed curve) is also superposed on the final profiles to show changes over the 5 days. (b) Observed (open symbols) and predicted (solid symbols) elevation at two cross-shore locations (circles, x=240 m, location of maximum erosion and triangles, x=320 m, location of maximum accretion) for every 3 hr period between 10 Oct 2200 and 15 Oct 2200 hrs versus time.

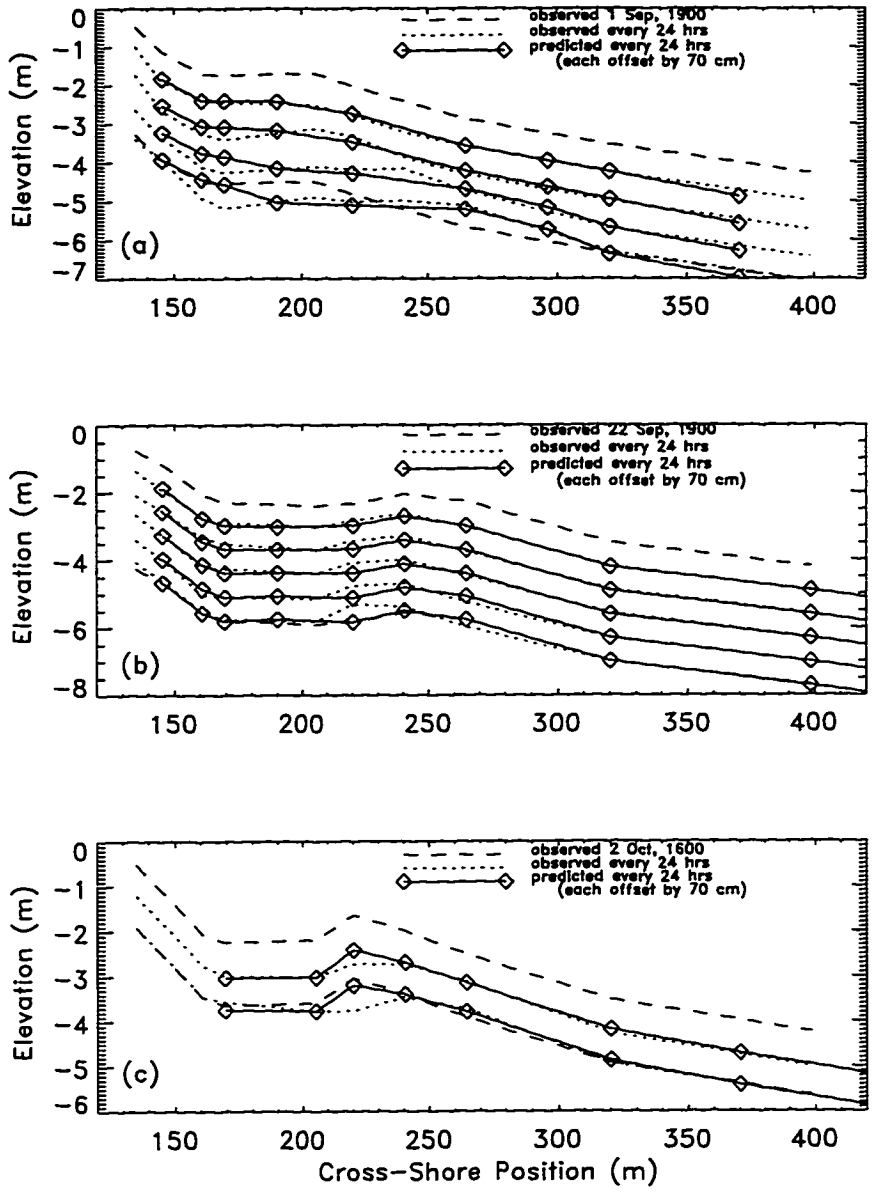

Figure 2.10: Observed (dotted curves) and predicted (solid curves with diamonds) elevation of the seafloor versus cross-shore position. Three-hour average profiles for each 24-hour period after model initialization are sequentially offset by -70 cm in the vertical. The initial profile (dashed curves) is superposed on the final profiles to show total profile changes. (a) 1 Sep 1900 - 5 Sep 2200 hrs, (b) 22 Sep 1900 - 27 Sep 2200 hrs, and (c) 2 Oct 1600 - 4 Oct 1300 hrs.

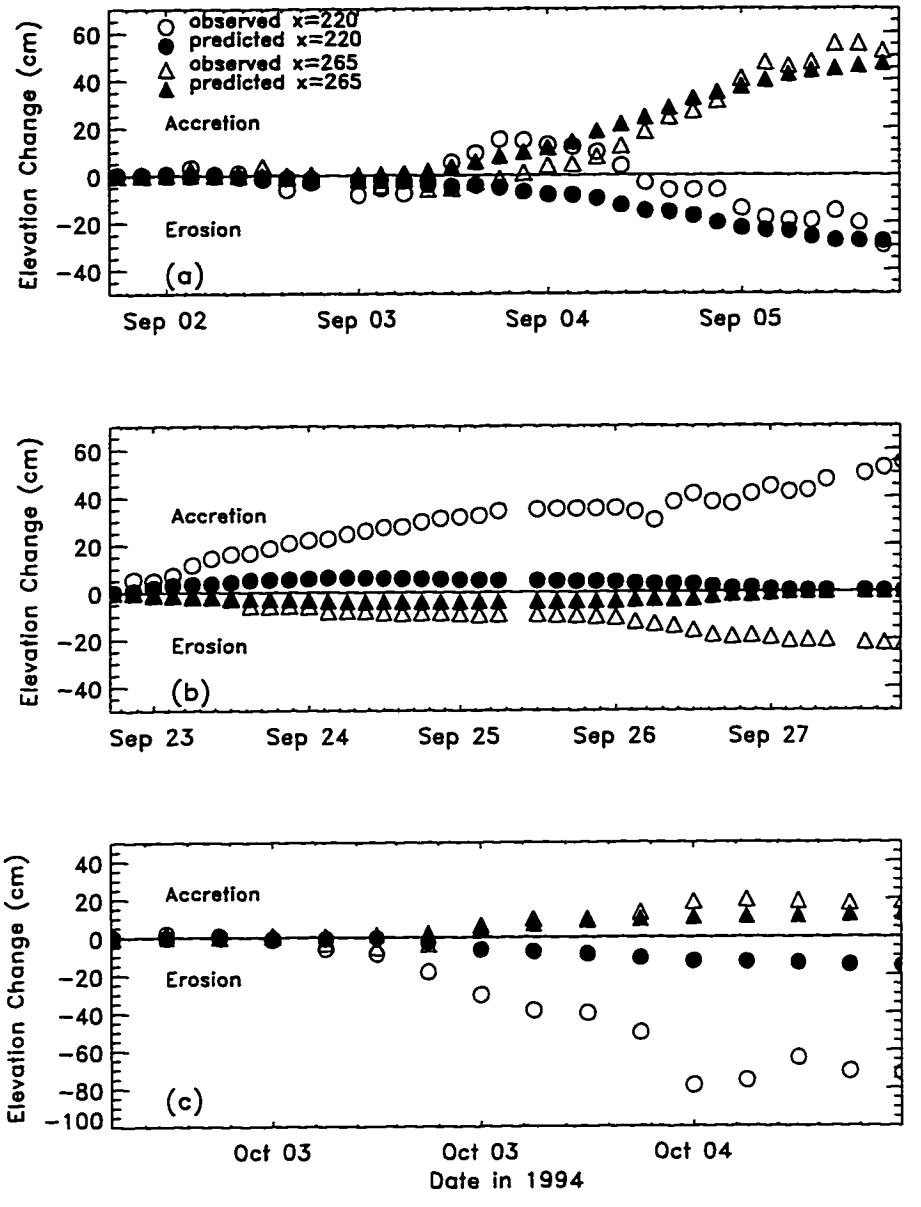

Figure 2.11: Observed (open symbols) and predicted (solid symbols) elevation at two cross-shore locations (triangles, x=265 m and circles, x=220) for each 3-hr period versus time. (a) 1 Sep 1900 – 5 Sep 2200 hrs, (b) 22 Sep 1900 – 27 Sep 2200 hrs, and (c) 2 Oct 1600 – 4 Oct 1300 hrs.

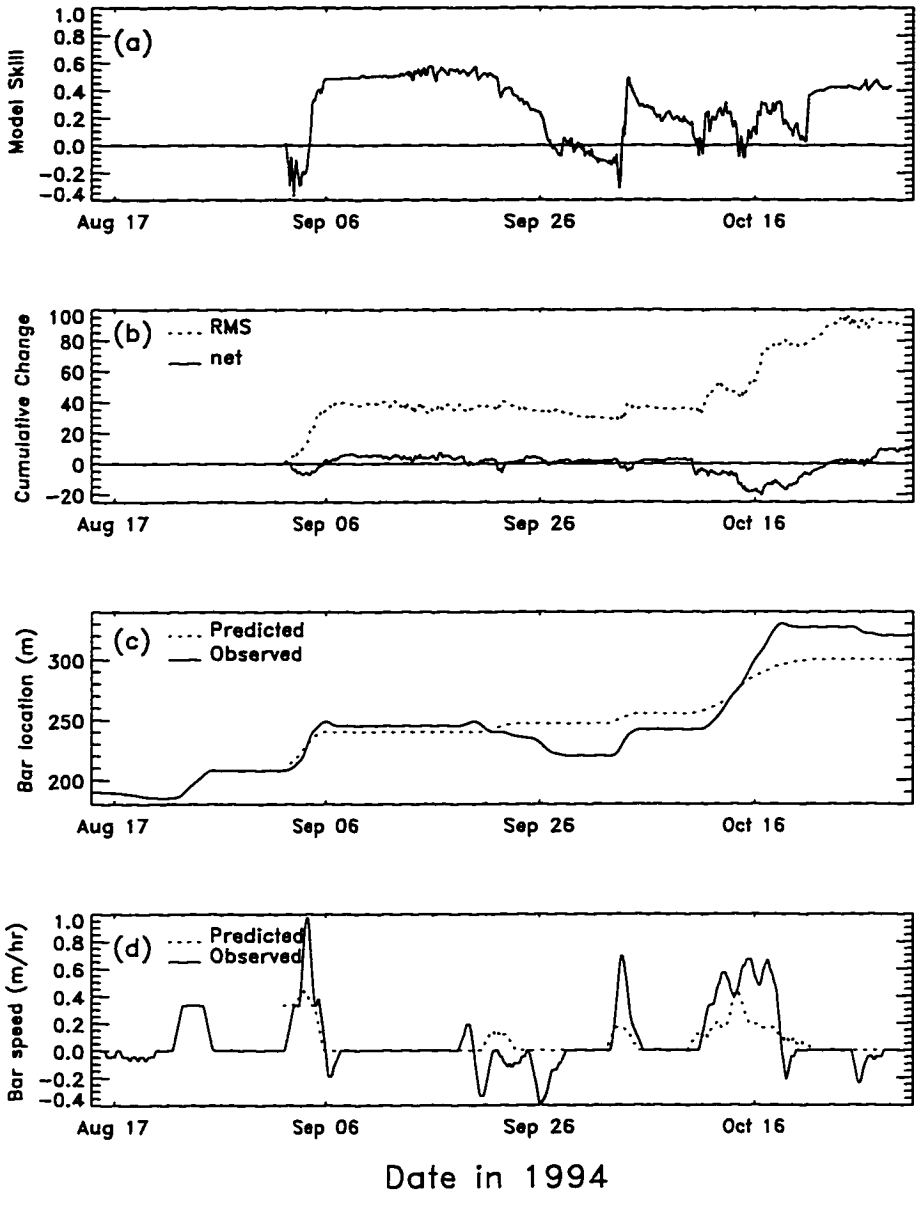

Figure 2.12: (a) Cumulative model skill, (b) observed RMS (dotted curve) and net (solid curve) total change, (c) predicted (dotted curve) and observed (solid curve) cross-shore location of the sand bar and (d) cross-shore migration speed of the sand bar versus time.

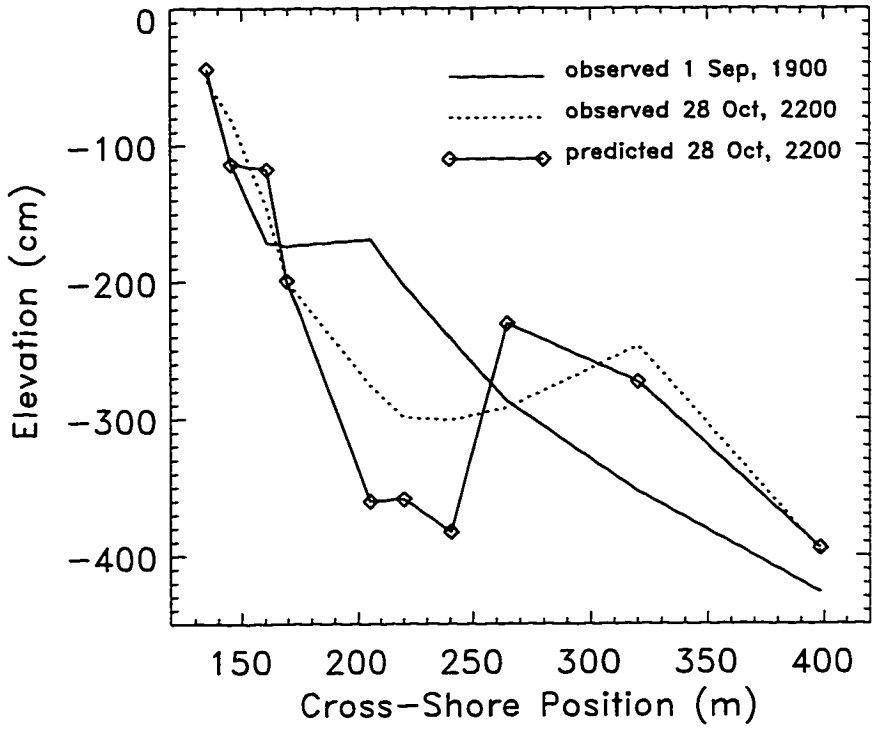

Figure 2.13: Observed (1 Sep 1900 hrs (initial condition), solid curve, and 28 Oct 2200 hrs, dotted curve) and predicted (28 Oct 2200 hrs, solid curve with diamonds) 3-hr average elevation of the seafloor versus cross-shore position.

Figure 2.14: Observed (open circles) and predicted (solid circles) change in seafloor elevation at four cross-shore locations for every 3-hr period between 1 Sep 1900 and 28 Oct 2200 hrs versus time. (a) x=170, (b) x=220, (c) x=265, and (d) x=320 m.

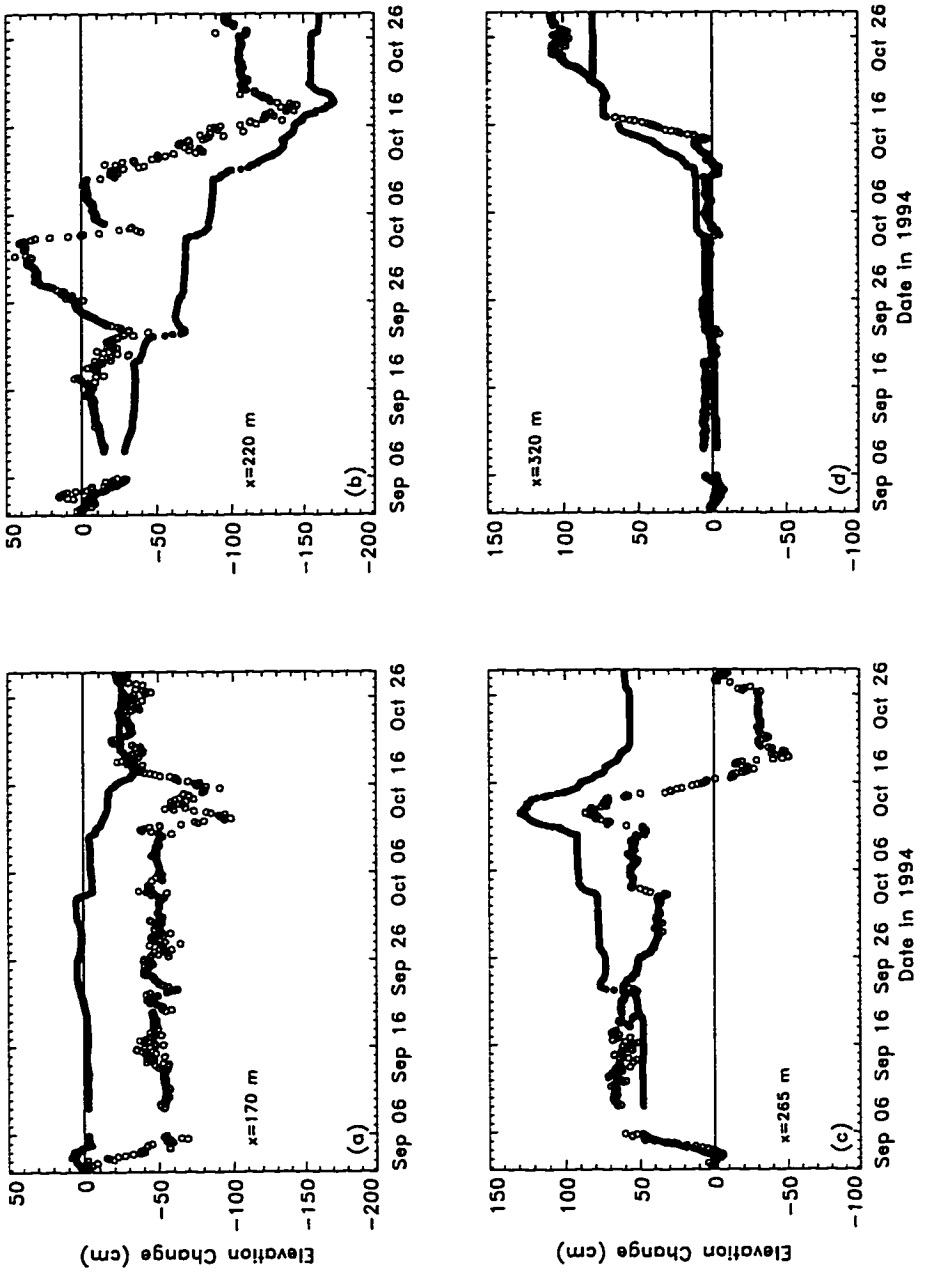

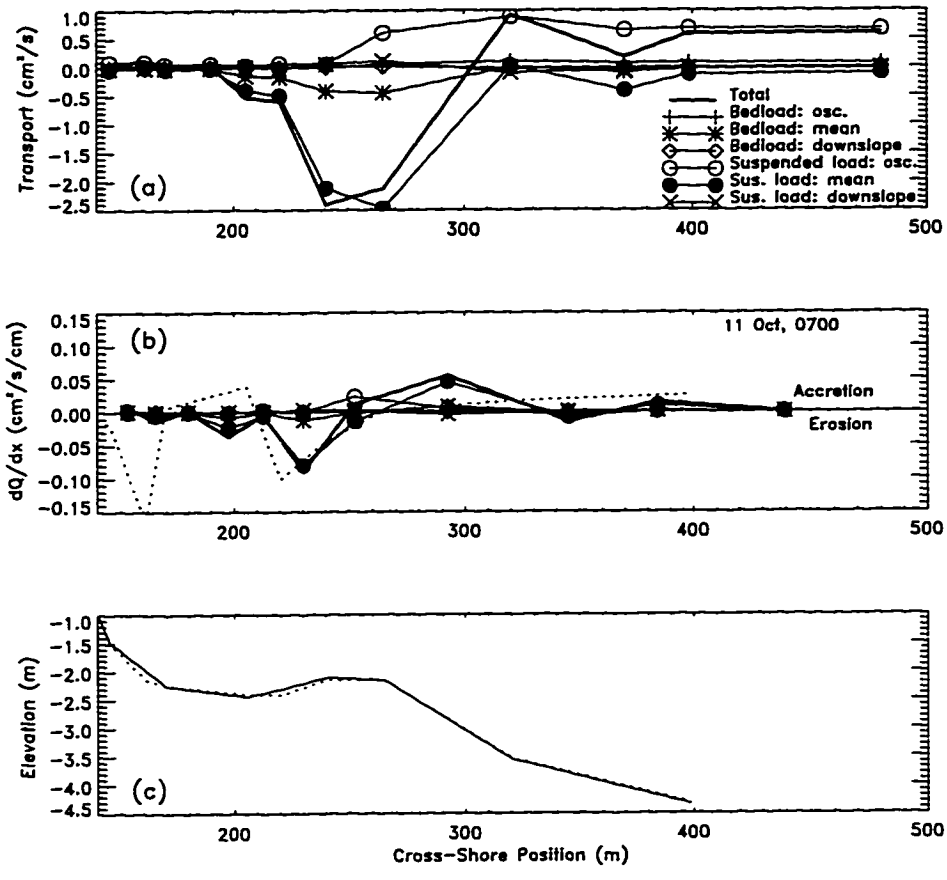

Figure 2.15: (a) Three-hour average predicted sediment transport for 11 Oct 0700–1000 hrs versus cross-shore position. The line types for transport predicted by each of the 6 terms in the model (3) are given in the legend and the thick solid curve is the total predicted transport. (b) Cross-shore gradients in each predicted transport term (same line types as (a)) and observed (dotted curve) total transport gradient. (c) Cross-shore profile observed 11 Oct 0700 hrs (solid curve) and 11 Oct 1000 hrs (dotted curve).

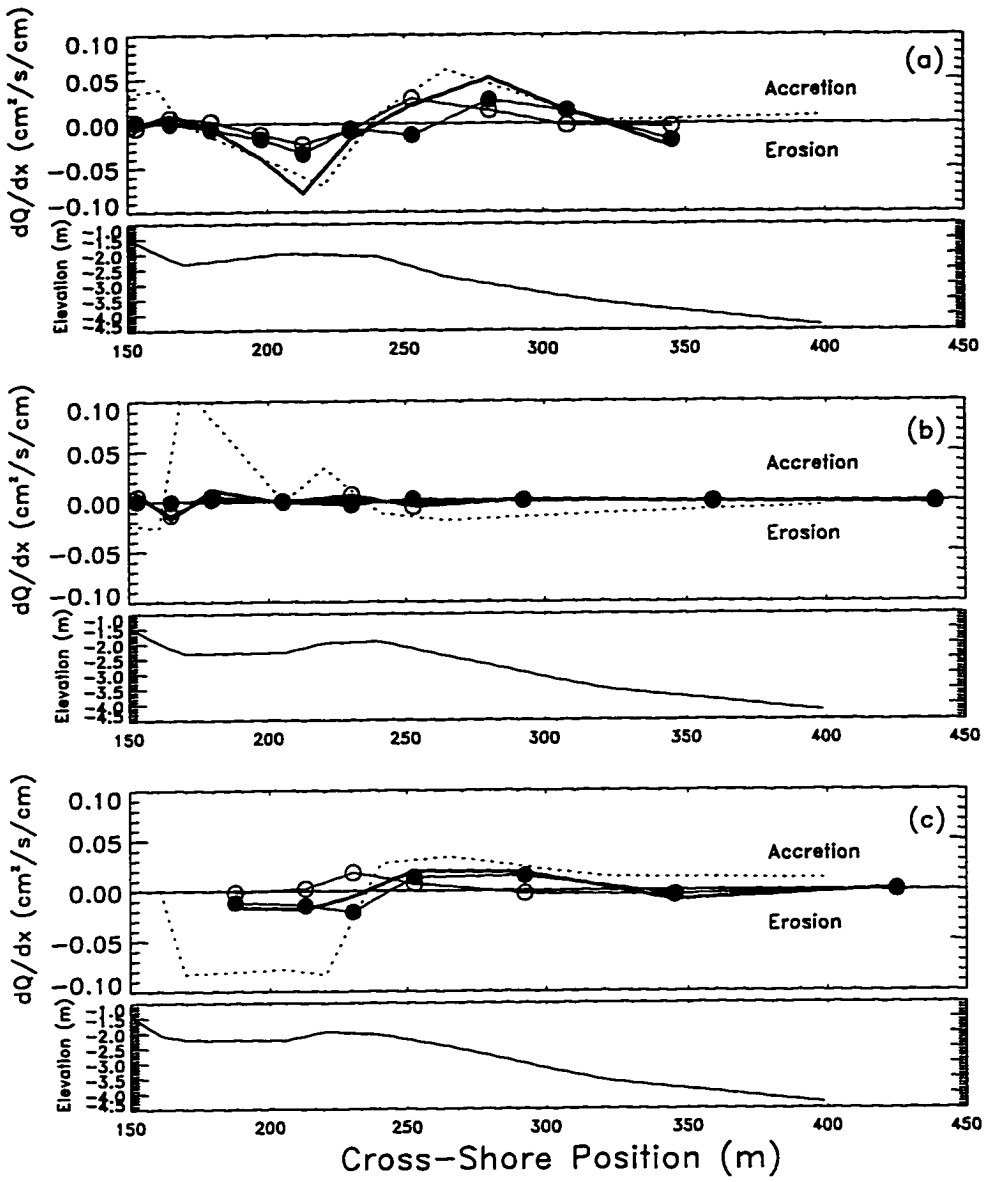

Figure 2.16: Three-hour average gradients in predicted mean- (solid circles) and oscillatory-flow-driven (open circles) suspended sediment transport, predicted total transport (thick solid curves), and observed transport (dotted curves). The corresponding cross-shore profile is shown in the bottom panels. (a) 4 Sep 1000–1300 hrs, (b) 26 Sep 1000–1300 hrs, and (c) 3 Oct 1900–2200 hrs.

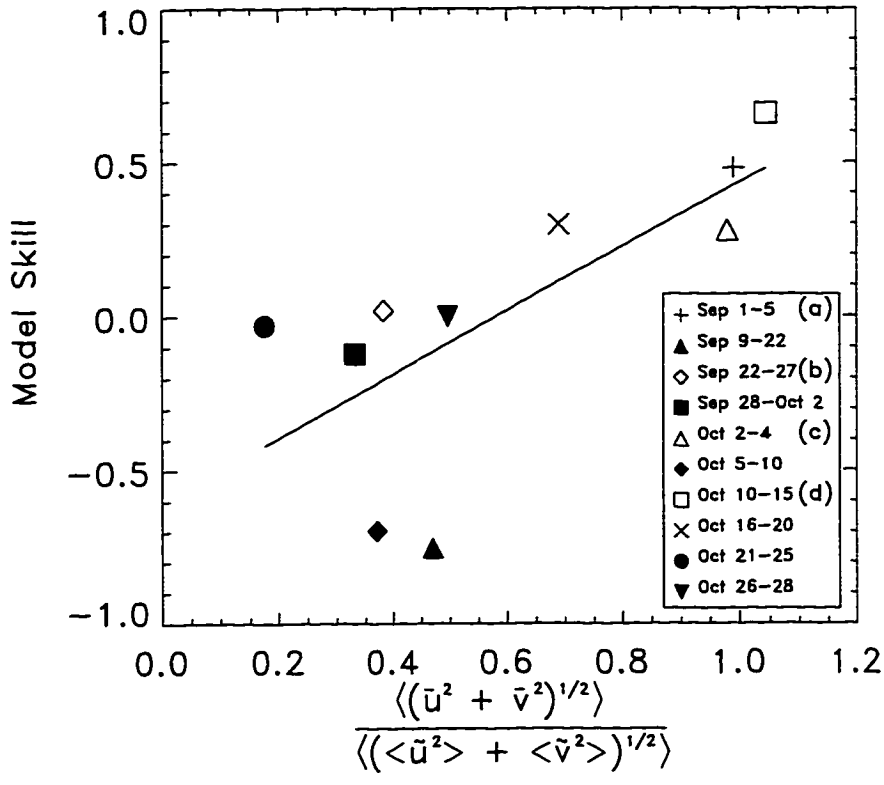

Figure 2.17: Model skill versus ratio of mean to RMS oscillatory flow. Solid filled symbols are periods of little or no bar migration. Open symbols are periods of largest profile change. The solid line is a least squares fit to all data points (r=0.7, significant at 95% level).

References

Aubrey, D.G., Seasonal Patterns of Onshore/Offshore Sediment Movement, *Journal of Geophysical Research* **84**, 6347–6354, 1979.

Bagnold, R.A., An Approach to the Sediment Transport Problem from General Physics, *U.S. Geological Survey Prof. Paper* **422-I**, 1966.

Bailard, J.A., An Energetics Total Load Sediment Transport Model for a Plane Sloping Beach, *Journal of Geophysical Research* **86**, 10938–10954, 1981.

Bailard, J.A., Modeling On-Offshore Sediment Transport in the Surf Zone, In: *Proc. 18th International Conf. on Coastal Engineering*, Cape Town, 1419–1438, 1982.

Bailard, J.A. and D.L. Inman, An Energetics Bedload Transport Model for a Plane Sloping Beach: Local Transport, *Journal of Geophysical Research* **86**, 2035–2043, 1981.

Bowen, A.J., Simple Models of Nearshore Sedimentation; Beach Profiles and Longshore Bars, *The Coastline of Canada* S.B. McCann, editor; Geological Survey of Canada Paper **80-10**, 1–11, 1980.

Bruun, P., Coast Erosion and the Development of Beach Profiles, U.S. Army Corps of Engineers, Beach Erosion Board, Tech. Memo. No. 44, 1954.

Church, J.C. and E.B. Thornton, Effects of Breaking Wave Induced Turbulence Within a Longshore Current Model, *Coastal Engineering* **20**, 1–28, 1993.

Clifton, H.E., Wave-Formed Sedimentary Structures-A Conceptual Model, in Davis and Ethington ed: *Beach and Nearshore Sedimentation, SEPM Special Publication* **24**, 126–148, 1976.

Dally, W.R. and R.G. Dean, Suspended Sediment Transport and Beach Profile Evolution, *Journal of Waterways, Port, Coastal, Ocean Engineering* **110**, 15–33, 1984.

Dean, R.G., Equilibrium Beach Profiles: US Atlantic and Gulf Coasts, Univ. of Delaware, Dept. of Civil Engineering, Ocean Engineering Report No. 12, 1977.

Dyhr-Nielsen, M. and T. Sorensen, Sand Transport Phenomena on Coasts With Bars, In: *Proc. 12th International Conf. on Coastal Engineering*, Washington DC, 855–866, 1970.

Eagleson, P.S. and R.G. Dean, Wave-Induced Motion of Bottom Sediment Particles, *ASCE Transactions* **126**, 1162–1189, 1961.

Fredsøe, J. and R. Diegaard, *Mechanics of Coastal Sediment Transport*, Advanced Series on Ocean Engineering, Vol.3, World Scientific, London, pp 369, 1992.

Gallagher, E.L., W. Boyd, S. Elgar, R.T. Guza, and B. Woodward, Performance of a Sonar Altimeter in the Nearshore, *Marine Geology* **133**, 241–248, 1996.

Haines, J.W. and A.H. Sallenger, Vertical Structure of Mean Cross-Shore Currents Across a Barred Surf Zone, *Journal of Geophysical Research* **99**, 14223–14242, 1994.

Hallermeier, R., Oscillatory Bedload Transport: Data Review and Simple Formulation, *Continental Shelf Research* **1**, 159–190, 1982.

Hanes, D.M. and D.A. Huntley, Continuous Measurements of Suspended Sand Concentration in a Wave Dominated Nearshore Environment, *Continental Shelf Research* **6**, 585–596, 1986.

Hay, A.E. and D.J. Wilson, Rotary Sidescan Images of Nearshore Bedform Evolution During a Storm, *Marine Geology* **119**, 1994.

Holman, R.A. and A.J. Bowen, Bars, Bumps and Holes: Models for the Generation of Complex Beach Topography, *Journal of Geophysical Research* **87**, 457–468, 1982.

Holman, R.A. and A.H. Sallenger, Sand Bar Generation: A Discussion of the Duck Experiment Series, *Journal of Coastal Research* Special Issue No. **15**, 76–92, 1993.

Inman, D.L. and A.J. Bowen, Flume Experiments on Sand Transport by Waves and Currents, In: *Proc. 8th International Conf. on Coastal Engineering*, Mexico City, 137–150, 1963.

Jaffe, B.E., R.W. Sternberg, and A.H. Sallenger, The Role of Suspended Sediment in Shore-Normal Beach Profile Changes, In: *Proc. 19th International Conf. on Coastal Engineering*, Houston, 1983–1996, 1984.

Kraus, N.G. and M. Larson, Prediction of Initial Profile Adjustment of Nourished Beaches to Wave Action, In: *Proc. Beach Technology '88*, Florida Shore and Beach Preservation Association, 125–137, 1988.

Kriebel, D.L. and R.G. Dean, Numerical Simulations of Time-Dependent Beach and Dune Erosion, *Coastal Engineering* **9**, 221–245, 1985.

Lee, G. and W. A. Birkemeier, Beach and Nearshore Survey Data: 1985–1991 CERC Field Research Facility, US Army Corps of Eng, Waterways Exp Station, Technical Report CERC-93-3, 1993.

Lippmann, T.C. and R.A. Holman, The Spatial and Temporal Variability of Sand Bar Morphology, *Journal of Geophysical Research* **95**, 11575–11590, 1990.

Lippmann, T.C., E.B. Thornton, and A.J.H.M. Reniers, Wave Stress and Longshore Current on Barred Profiles, In: *Proc. Coastal Dynamics '95*, Gdansk, 401–412, 1996.

Masselink, G. and K.P. Black, Magnitude and Cross-Shore Distribution of Bed Return Flow Measured on Natural Beaches, *Coastal Engineering* **25**, 165–190, 1995.

Middleton, G.V. and J.B. Southard, Mechanics of Sediment Movement. Lecture notes for short course no. 3, Society of Economic Paleontologists and Mineralogists, pp 401, 1982.

Nairn, R.B. and H.N. Southgate, Deterministic Profile Modeling of Nearshore Processes. Part 2. Sediment Transport and Beach Profile Development, *Coastal Engineering* **19**, 57–96, 1993.

Nielsen, P., *Coastal Bottom Boundary Layers and Sediment Transport*, Advanced Series on Ocean Engineering, Vol.4, World Scientific, London, pp 324, 1992.

Raudkivi, A.J. *Loose Boundary Hydraulics 3rd Edition*, Pergamon Press, New York, 1990.

Roelvink, J.A. and I. Brøker, Cross-Shore Profile Models, *Coastal Engineering* **21**, 163–191, 1993.

Roelvink, J.A. and M.J.F. Stive, Bar Generating Cross Shore Flow Mechanisms on a Beach, *Journal of Geophysical Research* **94**, 4785–4800, 1989.

Sallenger, A.H. and P.A. Howd, Nearshore Bars and the Break-Point Hypothesis, *Coastal Engineering* **12**, 301–313, 1989.

Sato, S. and N. Mitsunobu, A Numerical Model of Beach Profile Change Due to Random Waves. In: *Proc. ASCE Specialty Conf. Coastal Sediments '91*, Seattle, WA, 674–687, 1991.

Seymour, R.J., Nearshore Auto-Suspending Turbidity Flows, *Ocean Engineering* **13**, 435–447, 1986.

Seymour, R.J., An Assessment of NSTS, In: *Proc. of Coastal Sediments '87*, ASCE, New Orleans, LA, 642–651, 1987.

Sleath, J.F.A., *Sea Bed Mechanics*, John Wiley and sons, New York, 1984.

Smith, J.M., I.A. Svendsen and U. Petrevu, Vertical Structure of the Nearshore Current at Delilah: Measured and Modeled, In: *Proc. 23rd International Conf. on Coastal Engineering*, Venice, 2825–2838, 1992.

Stauble, D.K., Long-Term Profile and Sediment Morphodynamics: Field Research Facility Case History, Army Corps of Engineers Technical Report CERC-92-7, 1992.

Stive, M.J.F., A Model for Cross-Shore Sediment Transport. In: *Proc. 20th International Conf. on Coastal Engineering*, Taipei, 1550–1564, 1986.

Stive, M.J.F. and J.A. Battjes, A Model for Offshore Sediment Transport, In: *Proc. 19th International Conf. on Coastal Engineering*, Houston, 1420–1436, 1984.

Stive, M.J.F. and H.G. Wind, Cross-Shore Mean Flow in the Surf Zone, *Coastal Engineering* **6**, 1–25, 1986.

Svendsen, I.A. and J. Buhr Hansen, Cross-Shore Currents in Surf-Zone Modelling, *Coastal Engineering* **12**, 23–42, 1988.

Takeda, I., and T. Sunamura, Beach Changes by Storm Waves, In: *Proc. 20th International Conf. on Coastal Engineering*, Taipei, 1612–1622, 1987.

Thornton, E.B., R.T. Humiston, and W. Birkemeier, Bar/Trough Generation on a Natural Beach, *Journal of Geophysical Research* **101**, 12097–12110, 1996.

Watanabe, A. and M. Dibajnia, Numerical Modeling of Nearshore Waves, Cross Shore Sediment Transport and Beach Profile Change, In: *Proc. IAHR Symp. on Mathematical Modeling of Sediment Transport in the Coastal Zone*, Copenhagen, 166-174, 1988.

Winant, C.D., D.L. Inman, and C.E. Nordstrom, Description of Seasonal Beach Changes Using Empirical Eigenfinctions, *Journal of Geophysical Research* **80**, 1979–1986, 1975.

Wright, L.D. and A.D. Short, Morphodynamic Variability of Surf Zones and Beaches: a Synthesis, *Marine Geology* **26**, 93–118, 1984.